



## Technical note: The CAMS greenhouse gas reanalysis from 2003 to 2020

Anna Agustí-Panareda<sup>1</sup>, Jérôme Barré<sup>2</sup>, Sébastien Massart<sup>1</sup>, Antje Inness<sup>1</sup>, Ilse Aben<sup>3</sup>, Melanie Ades<sup>1</sup>, Bianca C. Baier<sup>4,5</sup>, Gianpaolo Balsamo<sup>1</sup>, Tobias Borsdorff<sup>3</sup>, Nicolas Bousquet<sup>1</sup>, Souhail Boussetta<sup>1</sup>, Michael Buchwitz<sup>6</sup>, Luca Cantarello<sup>1</sup>, Cyril Crevoisier<sup>7</sup>, Richard Engelen<sup>1</sup>, Henk Eskes<sup>8</sup>, Johannes Flemming<sup>1</sup>, Sébastien Garrigues<sup>1</sup>, Otto Hasekamp<sup>3</sup>, Vincent Huijnen<sup>8</sup>, Luke Jones<sup>1</sup>, Zak Kipling<sup>1</sup>, Bavo Langerock<sup>9</sup>, Joe McNorton<sup>1</sup>, Nicolas Meilhac<sup>7</sup>, Stefan Noël<sup>6</sup>, Mark Parrington<sup>1</sup>, Vincent-Henri Peuch<sup>1</sup>, Michel Ramonet<sup>10</sup>, Miha Razinger<sup>1</sup>, Maximilian Reuter<sup>6</sup>, Roberto Ribas<sup>1</sup>, Martin Sutcliffe<sup>1</sup>, Colm Sweeney<sup>5</sup>, Jérôme Tarniewicz<sup>10</sup>, and Lianghai Wu<sup>11</sup>

<sup>1</sup>European Centre for Medium Range Weather Forecasts, Shinfield Park, Reading RG2 9AX, United Kingdom

<sup>2</sup>Joint Center for Satellite Data Assimilation, University Corporation for Atmospheric Research,  
Boulder, CO, USA

<sup>3</sup>SRON Netherlands Institute for Space Research, Utrecht, the Netherlands

<sup>4</sup>Cooperative Institute for Research in Environmental Sciences,  
University of Colorado Boulder, Boulder, CO, USA

<sup>5</sup>NOAA, Global Monitoring Laboratory, Boulder, CO, USA

<sup>6</sup>Institute of Environmental Physics (IUP), University of Bremen, 28334 Bremen, Germany

<sup>7</sup>Laboratoire de Météorologie Dynamique (LMD/IPSL), CNRS,  
Ecole polytechnique, 91128 Palaiseau CEDEX, France

<sup>8</sup>Royal Netherlands Meteorological Institute, Utrechtseweg 297, 3731 GA De Bilt, the Netherlands

<sup>9</sup>Royal Belgian Institute for Space Aeronomy, Avenue Circulaire 3, 1180 Uccle, Belgium

<sup>10</sup>Laboratoire des Sciences du Climat et de l'Environnement (LSCE/IPSL), CEA-CNRS-UVSQ,  
Université Paris-Saclay, 91191 Gif-sur-Yvette, France

<sup>11</sup>Remote Sensing Unit, Flemish Institute for Technological Research (VITO),  
Boeretang 200, 2400 Mol, Belgium

**Correspondence:** Anna Agustí-Panareda (anna.agusti-panareda@ecmwf.int)

Received: 30 April 2022 – Discussion started: 18 July 2022

Revised: 26 January 2023 – Accepted: 16 February 2023 – Published: 31 March 2023

**Abstract.** The Copernicus Atmosphere Monitoring Service (CAMS) has recently produced a greenhouse gas reanalysis (version egg4) that covers almost 2 decades from 2003 to 2020 and which will be extended in the future. This reanalysis dataset includes carbon dioxide (CO<sub>2</sub>) and methane (CH<sub>4</sub>). The reanalysis procedure combines model data with satellite data into a globally complete and consistent dataset using the European Centre for Medium-Range Weather Forecasts' Integrated Forecasting System (IFS). This dataset has been carefully evaluated against independent observations to ensure validity and to point out deficiencies to the user. The greenhouse gas reanalysis can be used to examine the impact of atmospheric greenhouse gas concentrations on climate change (such as global and regional climate radiative forcing), assess intercontinental transport, and serve as boundary conditions for regional simulations, among other applications and scientific uses. The caveats associated with changes in assimilated observations and fixed underlying emissions are highlighted, as is their impact on the estimation of trends and annual growth rates of these long-lived greenhouse gases.

## 1 Introduction

Atmospheric carbon dioxide ( $\text{CO}_2$ ) and methane ( $\text{CH}_4$ ) are the most abundant anthropogenic greenhouse gases directly responsible for climate change (IPCC, 2021). Their long lifetime and increasing anthropogenic emissions near the surface account for their long-term trends (Friedlingstein et al., 2022). A lot of effort has been devoted to measuring the atmospheric concentrations from ground-based observatories, e.g. the National Oceanic and Atmospheric Administration (NOAA, <https://gml.noaa.gov>, last access: 18 March 2023) and the Integrated Carbon Observation System (ICOS, <https://www.icos-cp.eu>, last access: 18 March 2023), which provide the gold standard for the estimation of trends, and more recently satellite data (Committee on Earth Observation Satellites, CEOS; Crisp et al., 2018), enhancing the spatial coverage of greenhouse gas observations at the global scale. Atmospheric measurements also sample the variability of  $\text{CO}_2$  and  $\text{CH}_4$  coming from the weather and its associated atmospheric transport (e.g. Patra et al., 2008, 2011). For this reason, numerical weather prediction (NWP) models have been extensively used to represent and reconstruct the variability of atmospheric concentrations of various tracers (e.g. Inness et al., 2019). Here we use the Integrated Forecasting System (IFS) of the European Centre for Medium-Range Weather Forecasts (ECMWF), which has been adapted to include  $\text{CO}_2$  and  $\text{CH}_4$  in the weather forecast (Agustí-Panareda et al., 2017, 2019), to create a greenhouse gas (GHG) reanalysis. The reanalysis uses the data assimilation technique to combine  $\text{CO}_2$  and  $\text{CH}_4$  satellite data from the SCanning Imaging Absorption spectroMeter for Atmospheric CHartographY (SCIAMACHY, <https://www.sciamachy.org>, last access: 18 March 2023), the Infrared Atmospheric Sounding Interferometer (IASI, <https://www.eumetsat.int/iasi>, last access: 18 March 2023), and the Thermal and Near Infrared Sensor for Carbon Observation (TANSO, [https://www.eorc.jaxa.jp/GOSAT/instrument\\_1.html](https://www.eorc.jaxa.jp/GOSAT/instrument_1.html), last access: 18 March 2023) instruments with IFS model simulations of  $\text{CO}_2$  and  $\text{CH}_4$  (Agustí-Panareda et al., 2022). The dataset is based on a consistent and stable model version to provide a homogeneous, continuous and gapless record of the  $\text{CO}_2$  and  $\text{CH}_4$  in the entire atmosphere since 2003.

The IFS includes a combined forecasting model and data assimilation system. The data assimilation system also integrates meteorological observations, as in the fifth generation of ECMWF meteorological reanalyses, ERA5 (Hersbach et al., 2020), to best constrain the atmospheric variability of greenhouse gases (Massart et al., 2014, 2016). The forecasting model provides a three-dimensional representation and evolution of the atmospheric  $\text{CO}_2$  and  $\text{CH}_4$  and meteorological variables (Agustí-Panareda et al., 2019). At the model surface, the greenhouse gases are forced by a set of surface fluxes and emissions. Such modelling configuration allows us to produce a realistic representation of the spatio-temporal variability of greenhouse gases in the atmosphere over a wide

range of scales from hours to seasons and from local to global scales (Agustí-Panareda et al., 2022).

Figure 1 showcases the global evolution of  $\text{CO}_2$  and  $\text{CH}_4$  represented by the CAMS GHG reanalysis dataset over the period 2003–2020 and the span of the used satellite data. The seasonal averages illustrate the spatial and temporal variability information contained in the reanalysis dataset that can be exploited for a range of applications in atmospheric sciences. A key potential use of the CAMS GHG reanalysis is to assess the impact of greenhouse gases on climate change. The reanalysis three-dimensional fields could be used to investigate global and regional climate radiative forcing (e.g. <https://atmosphere.copernicus.eu/climate-forcing>, last access: 18 March 2023), serve as boundary conditions for regional simulations, assess intercontinental transport, and generally provide a reference for any other study focusing on atmospheric variability of  $\text{CO}_2$  and  $\text{CH}_4$ . However, care should be taken when using the CAMS GHG reanalysis to estimate trends and annual growth rates of these long-lived greenhouse gases by considering the caveats associated with the changes in the satellite retrievals of  $\text{CO}_2$  and  $\text{CH}_4$  and the fact that neither anthropogenic emissions nor natural fluxes are adjusted by the data assimilation system, unlike atmospheric inversions (e.g. Chevallier et al., 2019).

The objective of this technical report is to document the technical aspects of the method and input data used to produce the CAMS GHG reanalysis and to provide guidance to potential users on the strengths and limitations of the dataset. Section 2 describes the processing chain to produce the reanalysis and its components. Section 3 focuses on the evaluation of the CAMS GHG reanalysis using independent observations from the TCCON and NDACC networks, as well as surface in situ networks and AirCore profiles. A list of limitations and caveats of the CAMS GHG reanalysis associated with the changes in the assimilated data and the underlying model errors is compiled in Sect. 4. Finally, Sect. 5 provides a summary and outlook for future CAMS GHG reanalyses.

## 2 Methods

This section gives an overview of the different building blocks of the CAMS GHG reanalysis and the processing chain that integrates the different components to produce the reanalysis dataset.

### 2.1 The reanalysis cycling chain

The reanalysis production chain is illustrated in Fig. 2. It is a cycling procedure based on a 12 h data assimilation window that involves four main parts:

- The first part consists of satellite retrievals of  $\text{CO}_2$  and  $\text{CH}_4$  (see Sect. 2.2), as well as NWP observations (Hersbach et al., 2020).

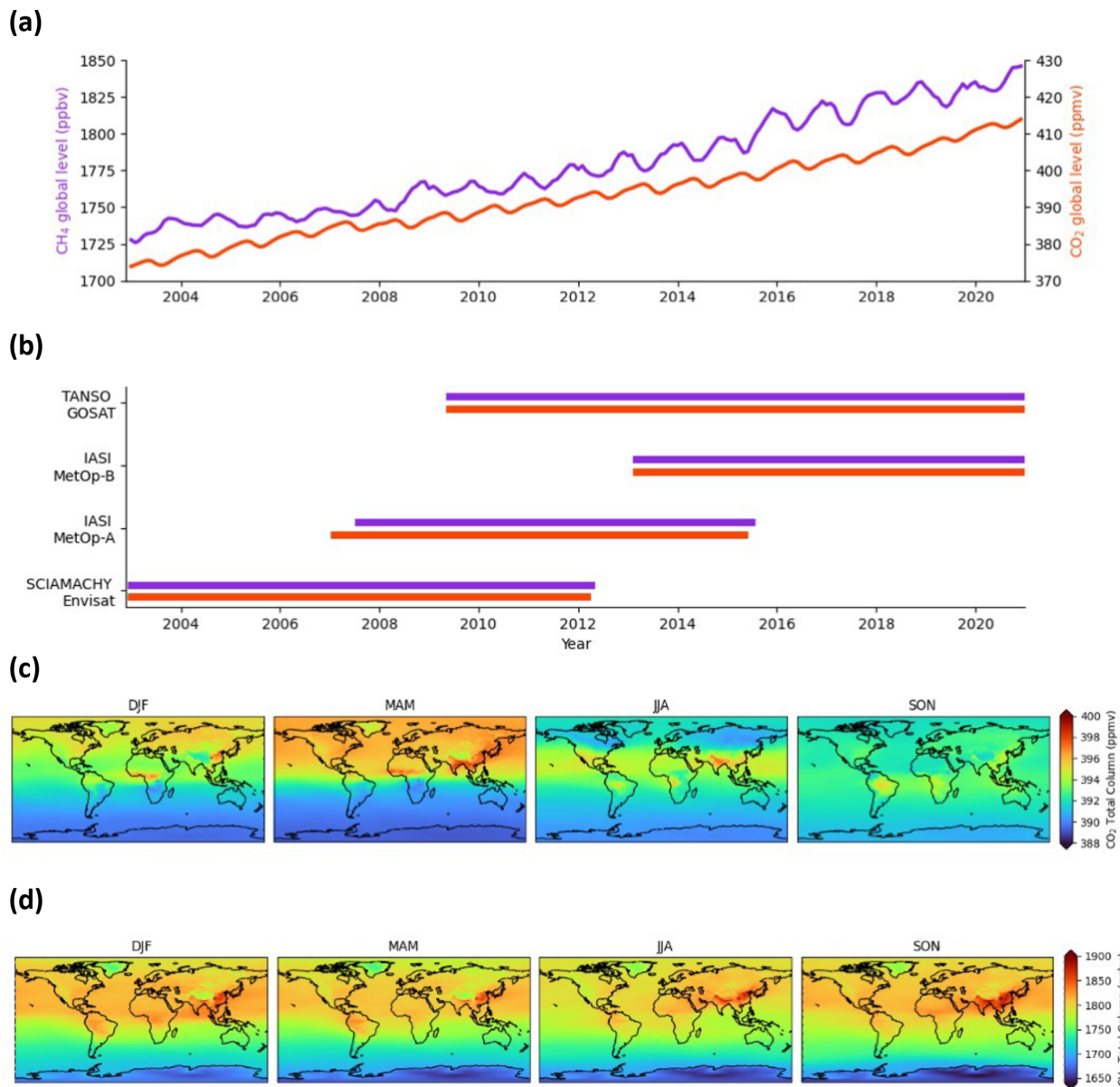


**Figure 1.** (a) Reanalysis time series of global column-averaged CO<sub>2</sub> (red) and CH<sub>4</sub> (purple) atmospheric mole fractions (global mean error ranges from −0.7 to +3.5 ppm based on evaluation in Sect. 3.3). (b) The span of the satellite data records for the corresponding species. (c) CO<sub>2</sub> and (d) CH<sub>4</sub> seasonal total column averages (DJF: December–January–February; MAM: March–April–May; JJA: June–July–August; SON: September, October, November) for the 2003–2020 period that illustrate the typical seasonal cycle. Note that individual years can be affected by the large inter-annual variability of biogenic fluxes (e.g. during El Niño years).

- The second part consists of surface fluxes (see Sect. 2.3) that constitute the sources and sinks of CO<sub>2</sub> and CH<sub>4</sub> in the atmosphere compiled from various sources. They provide the surface boundary condition for the tracer transport model.
- The third part is a model forecast (see Sect. 2.4) that provides a four-dimensional representation of the state of the greenhouse gases over space and time, along with other meteorological variables, during the 12 h analysis

window (from 09:00 to 21:00 and 21:00 to 09:00 UTC). The forecasts are initialised with the previous analysis, except for the first forecast for the initial date, which is initialised with atmospheric molar fractions from the CAMS inversion dataset (Chevallier, 2020; Segers et al., 2020a).

- The final part combines the above elements using a data assimilation system (see Sect. 2.5) to produce an analysis (Massart et al., 2014, 2016). The analysis will serve

to initialise the following forecast over the subsequent 12-hourly cycle.

Details of these four different components of the reanalysis processing chain, as well as the approach followed to monitor the assimilation of CO<sub>2</sub> and CH<sub>4</sub> satellite data, are provided in the subsections below.

## 2.2 Satellite GHG observations

The satellite measurements of radiances (L1 data) are processed by satellite retrievals developed by various data providers to derive information on the total and partial atmospheric column of CO<sub>2</sub> and CH<sub>4</sub> dry mole fraction (L2 data). In the CAMS GHG reanalysis, only L2 products were used for CO<sub>2</sub> and CH<sub>4</sub>. With nadir-looking satellite instrument geometries the L2 data provide vertically integrated content with vertical sensitivity functions called either averaging kernels (when an optimal estimation approach is used; Rodgers, 2000) or weighting functions, which provide information on where the retrieval sensitivity is located along the vertical. The satellite products assimilated in this reanalysis are all provided with an averaging kernel and prior information or weighting functions (Massart et al., 2014, 2016). The rationale for selecting the CO<sub>2</sub> and CH<sub>4</sub> satellite products is based on the availability of operational data in near real time as the strategy is to extend the CAMS GHG reanalysis to the present by eventually running it at close to real time. Table 1 provides the specification for each of the assimilated satellite CO<sub>2</sub> and CH<sub>4</sub> products, selected as the state-of-the-art retrievals at the beginning of 2017, when the CAMS GHG reanalysis production started. All of the L2 satellite products are freely available from the Copernicus Climate Change Service (C3S) Copernicus Climate Data Store (Alos et al., 2019; <https://cds.climate.copernicus.eu/cdsapp#!/dataset/satellite-carbon-dioxide>, last access: 18 March 2023, for CO<sub>2</sub> and <https://cds.climate.copernicus.eu/cdsapp#!/dataset/satellite-methane>, last access: 18 March 2023, for CH<sub>4</sub>). The GHG reanalysis integrates the L2 GHG data from the following satellite instruments.

– **SCIAMACHY – Envisat.** The SCanning Imaging Absorption spectroMeter for Atmospheric CartographHY (SCIAMACHY) instrument on board the Envisat satellite was launched by the European Space Agency (ESA) in March 2002, and it was developed by a consortium involving the Netherlands Space Office, the German Aerospace Center and the Belgian Federal Science Policy Office. It measures radiance variations from the ultraviolet to the near-visible infrared. The GHG L2 products use the nadir spectra of reflected and scattered solar radiation in the near-infrared region. Satellite radiance observations in the near-infrared spectral region with the nadir-looking geometry are sensitive to changes in CO<sub>2</sub> and CH<sub>4</sub> down to the Earth's surface. The measurements provide total column information with sensi-

tivity peaking near the surface. The ground pixel size is typically between 30 and 60 km, and the swath width is about 960 km. There are no across-track gaps between the ground pixels, but there are gaps in the along-track direction as SCIAMACHY operates only part of the time (approx. 50 %) in nadir observation mode. The CO<sub>2</sub> and CH<sub>4</sub> column products are retrieved by the University of Bremen (Reuter et al., 2011) and the Netherlands Institute for Space Research (SRON) (Frankenberg et al., 2011), respectively. Both of the L2 products are delivered by the ESA GHG-Climate Change Initiative (CCI; Buchwitz et al., 2015) and the C3S Climate Data Store (<https://cds.climate.copernicus.eu>, last access: 18 March 2023).

– **TANSO-FTS – GOSAT.** The Thermal And Near infrared Sensor for carbon Observations – Fourier Transform Spectrometer (TANSO-FTS) instrument on board the Greenhouse Gases Observing Satellite (GOSAT) was developed by the Japan Aerospace Exploration Agency (JAXA) and launched in January 2009. TANSO-FTS measures radiances in the short-wave infrared band that provide information of total column CO<sub>2</sub> and CH<sub>4</sub> mole fractions. Similar to SCIAMACHY, the sensitivity of the total column information provided by L2 data peaks near the surface due to the spectral band used. The ground pixel size is about 10 km, the swath is 750 km, and it has a revisit time of 3 d. In contrast to SCIAMACHY, the GOSAT scan pattern consists of non-consecutive individual ground pixels; i.e. it is not a gap-free scan pattern. For a general overview about GOSAT, see <http://www.gosat.nies.go.jp/en/> (last access: 18 March 2023). The L2 retrieval product is engineered by the SRON (Schepers et al., 2012, 2016) and delivered by the ESA GHG-CCI and the C3S Climate Data Store (<https://cds.climate.copernicus.eu>).

– **IASI – Metop A and B.** The Infrared Atmospheric Sounding Interferometer (IASI) instruments are on board the Meteorological Operational satellites Metop-A and Metop-B, launched in October 2006 and September 2012, respectively. The French National Centre for Space Studies (CNES) led the design and development of the instruments in collaboration with the European Organisation for the Exploitation of Meteorological Satellites (EUMETSAT). The IASI instruments measure the thermal infrared band with high spectral resolution, enabling them to detect a wide range of trace gas variations in the atmosphere, including CO<sub>2</sub> and CH<sub>4</sub> sensitive in the middle- and upper-tropospheric regions between 5 and 12 km altitude. IASI is an across-track-scanning system with a swath width of 2200 km providing global coverage twice a day. The field of view is sampled by 2 × 2 pixels whose ground resolution is 12 km at nadir. Both

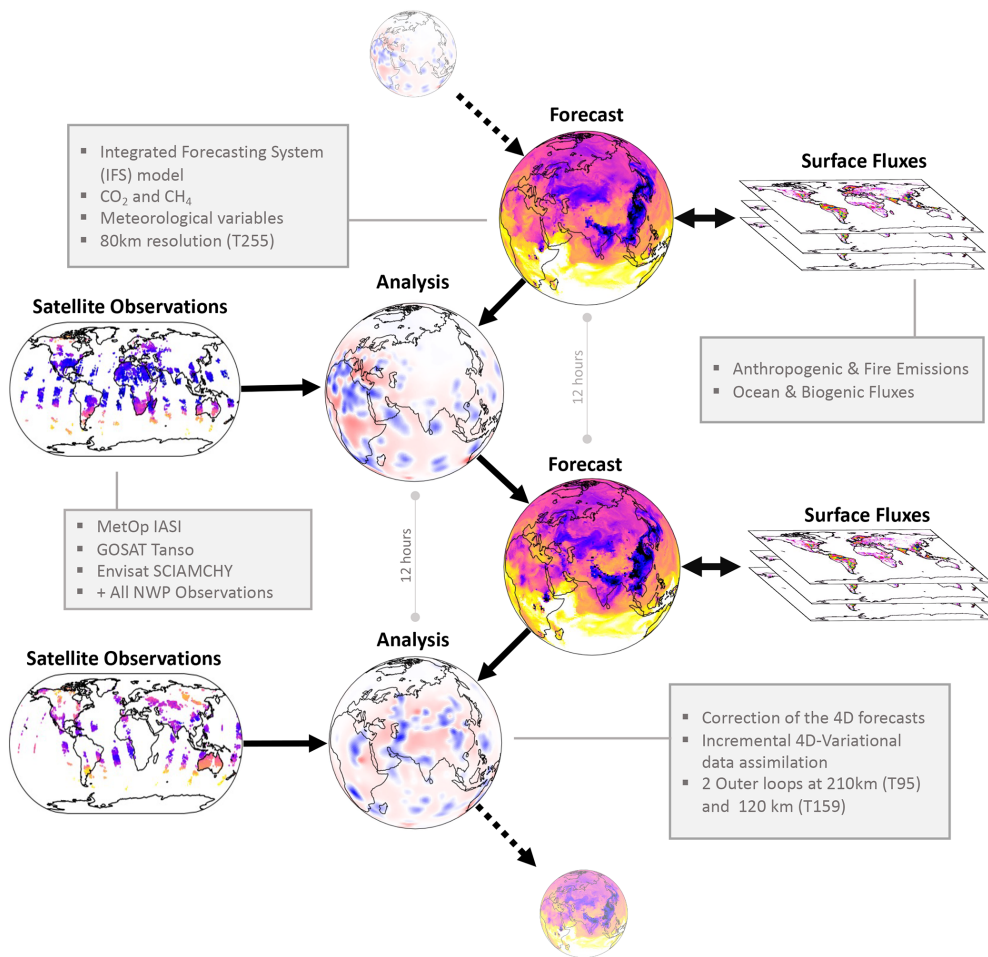


**Figure 2.** Schematic of the reanalysis cycling procedure. The flow diagram shows the steps and elements combined in the reanalysis. Surface fluxes are used as boundary condition for the atmospheric forecasts. Satellite data are combined with the forecast using data assimilation to produce an analysis (corrected 4D fields) to initialise the next forecast.

CO<sub>2</sub> and CH<sub>4</sub> are engineered and delivered by the Centre National de Recherche Scientifique (CNRS) Laboratoire de Météorologie Dynamique (LMD) (Crevoisier et al., 2009a, b, 2014). The two L2 products are delivered by the ESA GHG-Climate Change Initiative (Buchwitz et al., 2015) and the C3S Climate Data Store (<https://cds.climate.copernicus.eu>).

### 2.3 Surface fluxes and prescribed sources and sinks

The emissions and surface fluxes provide the surface boundary conditions for the atmospheric concentrations of CO<sub>2</sub> and CH<sub>4</sub>. They play a crucial role in determining the variability and growth rate of both greenhouse gases in the atmosphere. Errors in the budget of the total flux will result in systematic errors or biases in the forecast of atmospheric CO<sub>2</sub> and CH<sub>4</sub>. In the CAMS reanalysis, the surface fluxes (including sources and sinks) are not optimised by the assimilation system. This lack of surface flux optimisation can lead to biases

in the analysis when the observing system coverage is sparse in space and time or when the observation error is large, and the analysis is strongly influenced by the model forecast.

Table 2 lists the datasets used to produce the CAMS reanalysis, and Fig. 3 shows the seasonal cycle and trend of the global mean values of each type of surface flux used in the simulations. They include the following datasets.

- The first dataset includes fire emissions derived using the CAMS Global Fire Assimilation System (GFAS) version 1.2 that assimilate fire radiative power observations from satellite-based sensors (Kaiser et al., 2012). GFAS produces daily estimates of wildfire and biomass burning emissions. The emissions are injected at the surface and distributed over the boundary layer by the model's convection and vertical diffusion scheme.
- The second dataset includes anthropogenic emissions from the Emission Database for Global Atmospheric Research (EDGAR) version 4.2FT2010 in-

**Table 1.** Specifications of the satellite data used in the CAMS GHG reanalysis.

Gas	Instrument – satellite	Period assimilated (yyyymmdd)	Version (data provider)	Reference	Peaking sensitivity
CO <sub>2</sub>	SCIAMACHY – Envisat	20030101–20120324	CO <sub>2</sub> _SCI_BESD (v02.01.02, IUP-UB)	Reuter et al. (2011)	Near surface
	IASI – Metop-A	20070701–20150531	CO <sub>2</sub> _IAS_NLIS (v8.0, CNRS-LMD)	Crevoisier et al. (2009a)	Middle and upper troposphere
	IASI – Metop-B	20130201–20181130 20181201–20201231	CO <sub>2</sub> _IAS_NLIS (v4.2_nrt, CNRS-LMD) CO <sub>2</sub> _IAS_NLIS (v4.0_nrt, CNRS-LMD)		Middle and upper troposphere
TANSO-FTS – GOSAT		20090601–20131231	CO <sub>2</sub> _GOS_SRFP (V2.3.6, SRON)	Butz et al. (2011), Guerlet et al. (2013), Heymann et al. (2015)	Near surface
		20140101–20181231	CO <sub>2</sub> _GOS_SRFP (V2.3.8, SRON)		
		20190101–20201231	CO <sub>2</sub> _GOS_BESD (CAMS_NRT, IUP-UB)		
CH <sub>4</sub>	SCIAMACHY – Envisat	20030108–20100601	CH <sub>4</sub> _SCI_IMAP (v7.2, SRON)	Frankenberg et al. (2011)	Near surface
	IASI – Metop-A	20070701–20150630	CH <sub>4</sub> _IAS_NLIS (V8.3, CNRS-LMD)	Crevoisier et al. (2009b, 2014)	Middle and upper troposphere
	IASI – Metop-B	20130201–20181130 20181201–20201231	CH <sub>4</sub> _IAS_NLIS (V8.1_nrt, CNRS-LDM) CH <sub>4</sub> _IAS_NLIS (v4.0_nrt, CNRS-LDM)		Middle and upper troposphere
	TANSO-FTS – GOSAT	20090601–20131231 20140101–20181231 20190101–20201231	CH <sub>4</sub> _GOS_SRFP (V2.3.6, SRON) CH <sub>4</sub> _GOS_SRFP (V2.3.8, SRON) CH <sub>4</sub> _GOS_SRPR (CAMS_NRT, SRON)	Butz et al. (2010), Schepers et al. (2012)	Near surface

**Table 2.** Specifications of the emission and surface fluxes used in the CAMS GHG reanalysis.

Gas	Emission or flux type	Data provider – version
CO <sub>2</sub>	CO <sub>2</sub> and CH <sub>4</sub> fire emissions	GFAS Version 1.2 (Kaiser et al., 2012)
	CO <sub>2</sub> ocean fluxes	Takahashi climatology (Takahashi et al., 2009)
	CO <sub>2</sub> emissions from aviation	based on ACCMIP NO emissions from aviation scaled to annual total CO <sub>2</sub> from EDGAR aviation emissions (Olivier and Janssens-Maenhout, 2012)
	CO <sub>2</sub> ecosystem fluxes bias corrected with BFAS	based on CHTESSEL (modelled online in IFS) (Boussetta et al., 2013; Agustí-Panareda et al., 2016)
	CO <sub>2</sub> anthropogenic emissions	EDGARv4.2FT2010 (2003–2010) (Olivier and Janssens-Maenhout, 2012)
CH <sub>4</sub>	CH <sub>4</sub> total natural emissions	based on EDGARv4.2FT2010 (2003–2010) (Olivier and Janssens-Maenhout, 2012), LPJ-WHyMe wetland climatology (Spahni et al., 2011), and other natural sources and sinks (Matthews et al., 1991; Ridgwell et al., 1999; Houweling et al., 1999; Lambert and Schmidt, 1993; Sanderson, 1996)
	CH <sub>4</sub> chemical sink	monthly mean climatology of CH <sub>4</sub> loss rate from Bergamaschi et al. (2009)
	CH <sub>4</sub> anthropogenic emissions	EDGARv4.2FT2010 (2003–2010) (Olivier and Janssens-Maenhout, 2012)

ventory (Janssens-Maenhout et al., 2011; Olivier and Janssens-Maenhout, 2012) excluding the short carbon cycle. The anthropogenic emissions are based on annual average values and include emissions from fossil fuel combustion and leakage, agriculture, landfill and waste, and aviation, the latter being based on the Atmospheric Chemistry and Climate Model Intercompar-

ison Project (ACCMIP, Lamarque et al., 2013) nitric oxide (NO) emissions scaled to the annual CO<sub>2</sub> total emissions from aviation from EDGAR. EDGAR produces global anthropogenic emissions for both CO<sub>2</sub> and CH<sub>4</sub> at a relatively high resolution of 0.1° (compared to 80 km resolution of the CAMS reanalysis). The problem with EDGAR is that the latest version available at

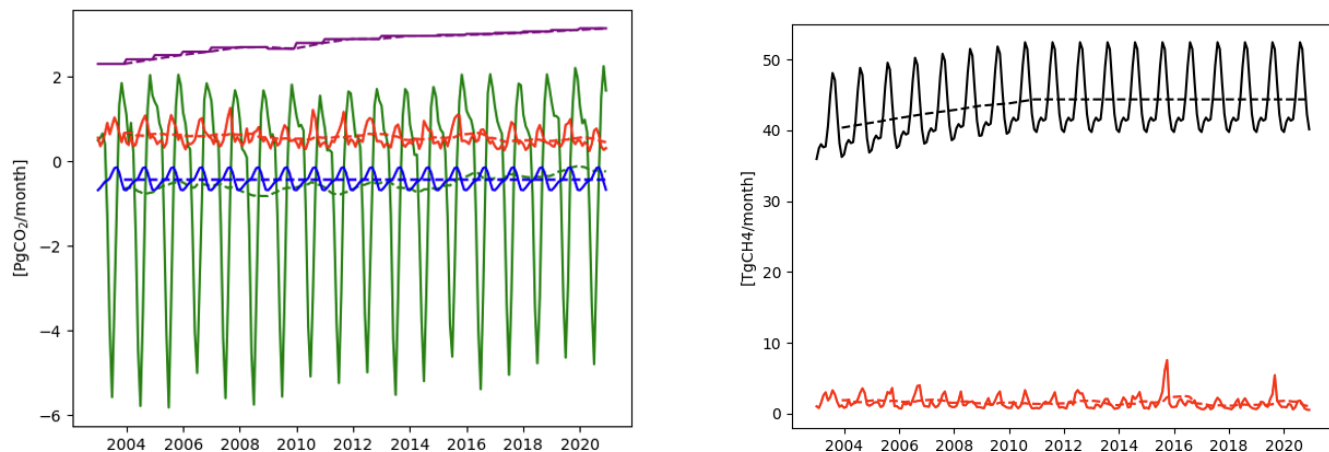


**Figure 3.** Monthly CO<sub>2</sub> and CH<sub>4</sub> surface fluxes. The CO<sub>2</sub> fluxes (Pg CO<sub>2</sub> per month) include modelled net ecosystem exchange (NEE) fluxes (in green), anthropogenic emissions (in purple), ocean fluxes (in blue) and biomass burning emissions (in red). The total CH<sub>4</sub> fluxes (Tg CH<sub>4</sub> per month) excluding biomass burning emissions are shown by the black line, and CH<sub>4</sub> biomass burning emissions (Tg CH<sub>4</sub> per month) are depicted with the red line. The dashed lines show the 1-year running mean for each of the fluxes.

the time when the CAMS reanalysis started does not extend beyond 2010. Anthropogenic emissions of CO<sub>2</sub> are extrapolated from 2010 to 2014 with the time series of country totals from EDGARv4.3 (Janssens-Maenhout et al., 2016), and from 2015 to 2020 a persistent growth based on the last available year (2014) is applied. CH<sub>4</sub> anthropogenic emissions are fixed with the last year of available gridded data (2010) from 2011 to 2020. Note that CO<sub>2</sub> and CH<sub>4</sub> emissions are not adjusted for the COVID-related emission reduction in 2020 (Le Quéré et al., 2020).

- The third dataset includes biogenic CO<sub>2</sub> fluxes that are based on the online CHTESSEL module (Boussetta et al., 2013), which relates CO<sub>2</sub> biogenic fluxes with radiation, precipitation, temperature, humidity and soil moisture. CHTESSEL is used in conjunction with the biogenic flux adjustment system (BFAS), which improves the continental budget of CO<sub>2</sub> fluxes by combining information from flux estimates of a global flux inversion system (Chevallier et al., 2010), land use information and CHTESSEL online fluxes (Agustí-Panareda et al., 2016). The two-way interaction between the atmospheric forecast and the surface fluxes depicts how the forecast influences the surface fluxes and vice versa via the coupling of the biogenic fluxes to the atmospheric forecast (radiation, temperature, humidity and soil moisture) and the influence of the resulting biogenic fluxes on the atmospheric CO<sub>2</sub> forecast.
- The fourth dataset includes wetland CH<sub>4</sub> monthly mean emissions that come from a climatology (1990–2008) based on the LPJ-WHyMe model, which is constrained by SCIAMACHY observations (Spanhi et al., 2011).

- The fifth dataset includes a monthly modulation for CH<sub>4</sub> rice emissions that is implemented based on the seasonal cycle of Matthews et al. (1991).
- The sixth dataset includes a CH<sub>4</sub> chemical sink that is represented by a monthly mean climatological loss rate from Bergamaschi et al. (2009) based on OH fields optimised with methyl chloroform (Bergamaschi et al., 2005; Houweling et al., 1998) and stratospheric radicals from the 2D photochemical Max Planck Institute (MPI) model (Brühl and Crutzen, 1993).
- Finally, the remaining datasets include a CH<sub>4</sub> monthly soil sink (Ridgwell et al., 1999), CO<sub>2</sub> and CH<sub>4</sub> annual mean oceanic fluxes (Houweling et al., 1999; Lambert and Schmidt, 1993; Takahashi et al., 2009), and CH<sub>4</sub> monthly mean fluxes from termites (Sanderson, 1996) and wild animals (Houweling et al., 1999).

#### 2.4 Forecast model

The CAMS GHG reanalysis has been produced using the IFS model. The same model is used to produce operational NWP at ECMWF, and the CAMS global forecast and analyses are used for reactive gas, aerosols and greenhouse gases at ECMWF (Fleming et al., 2015; Agustí-Panareda et al., 2017, 2022). The IFS model version used is IFS CY42R1, the same as in the CAMS reanalysis for reactive gases and aerosols (Inness et al., 2019). The forecasting model uses a reduced Gaussian grid with a resolution of TL255, corresponding to a horizontal resolution of approximately 80 km and 60 hybrid sigma-pressure vertical levels from the surface to 0.1 hPa. The tracer advection is computed using a non-mass-conserving, semi-implicit and semi-Lagrangian scheme (Temperton et al., 2001; Diamantakis and Magnus-

son, 2016). This scheme leads to an error growth that can dominate the signal in the model simulations if it is not corrected. Thus, a mass fixer is required to ensure mass conservation at every time step (Diamantakis and Agustí-Panareda, 2017). The mass fixer is particularly important for long-lived greenhouse gases for which the interesting signals to monitor, e.g. trends or annual growth rates and large-scale spatial gradients, are weak compared to the large background values. The transport model also includes a turbulent mixing scheme (Sandu et al., 2013) and a convection scheme (Bechtold et al., 2014). For the CH<sub>4</sub> chemical sink in the troposphere and the stratosphere, climatological loss rates derived from the Max Planck Institute photochemical model are used (Bergamaschi et al., 2009). Full documentation of the IFS can be found at <https://www.ecmwf.int/en/publications/ifs-documentation> (last access: 18 March 2023).

## 2.5 Analysis procedure (data assimilation)

The IFS system uses an incremental formulation of the four-dimensional variational technique (4D-Var). The 4D-Var technique consists of minimising a cost function that combines the model information and the observation information in order to obtain the best possible state of the atmosphere (analysis) accounting for the model and observation errors. The incremental 4D-Var cost function is quadratic and is formulated as follows:

$$J(\delta\mathbf{x}) = \frac{1}{2}(\delta\mathbf{x} - \delta\mathbf{x}_b)^T \mathbf{B}^{-1} (\delta\mathbf{x} - \delta\mathbf{x}_b) + \frac{1}{2}(\mathbf{G}\delta\mathbf{x} - \mathbf{d})^T \mathbf{R}^{-1} (\mathbf{G}\delta\mathbf{x} - \mathbf{d}), \quad (1)$$

where  $\delta\mathbf{x}$  is the increment, i.e. the difference between the model state  $\mathbf{x}$  and the first guess  $\mathbf{x}_g$ ,  $\delta\mathbf{x}_b$  is the difference between the background (the forecast started from the previous analysis) and the first guess,  $\mathbf{B}$  is the background error covariance matrix,  $\mathbf{R}$  is the observation error covariance matrix, and  $\mathbf{G}$  is the observation operator or forward operator that translates the information from model space to observation space. The innovation vector is  $\mathbf{d} = \mathbf{y} - \mathbf{G}\mathbf{x}_g$ , where  $\mathbf{y}$  is the observation vector and  $\mathbf{x}_g$  is the first guess. When the minimisation of the cost function is complete,  $\delta\mathbf{x}$  is added to  $\mathbf{x}_g$  to provide the analysis.

$$\mathbf{x}_a = \mathbf{x}_g + \delta\mathbf{x} \quad (2)$$

The analysis is performed over 12 h assimilation windows from 09:00 to 21:00 and from 21:00 to 09:00 UTC. The incremental 4D-Var assimilation involves the stepwise minimisation of the linearised cost function (Eq. 1) by updating the first guess  $\mathbf{x}_g$  and increasing the resolution. In the CAMS reanalysis setup, two minimisations are completed successively at TL95 (approximately 210 km) and TL159 (approximately 110 km) spectral truncations. Once the assimilation procedure is completed, an analysis is generated that will

serve to initialise the next forecast at the full TL255 resolution.

The background errors for CO<sub>2</sub> and CH<sub>4</sub> were produced from an ensemble of data assimilations (Massart et al., 2016), which allows the calculation of differences between pairs of background fields that have the characteristics of the background errors. The background errors for the greenhouse gas species are univariate, which means that there is no correlation between the greenhouse gas species and the dynamical fields. Hence, each species is assimilated independently of the others. The background errors used for both the greenhouse gas species and the dynamical fields are also constant in time. In the ECMWF data assimilation system, the background error covariance matrix is given in a wavelet formulation (Fisher, 2004, 2006). This allows both spatial and spectral variations of the horizontal and vertical background error covariances globally. Figure 4 shows the global mean of the standard deviation and average horizontal correlation length scales for both CH<sub>4</sub> and CO<sub>2</sub>. Following experimentation, the correlation length scales between the background errors were manually reduced in the atmospheric boundary layer (1 km from the surface).

## 2.6 Monitoring the data assimilation system

The time series of the departures (or differences) between the analysis (AN) and the assimilated satellite data (hereafter referred to as observations, OBS), as well as those between the underlying model simulation (or background, BG) and the OBS, are used to monitor the performance of the analysis system and are shown in Fig. 5 (for CO<sub>2</sub>) and Fig. 6 (for CH<sub>4</sub>). For each satellite retrieval product, both the BG departures (OBS–BG, green lines) and the AN departures (OBS–AN, red lines) are plotted (Figs. 5a and 6a: SCIAMACHY; Figs. 5b and 6b: IASI-A; Figs. 5c and 6c: IASI-B; Figs. 5d and 6d: GOSAT), together with the number of observations assimilated monthly (blue lines). Overall, both the random (i.e. standard deviation, dashed lines) and systematic components of the departures (i.e. average values, solid lines) are shown to be reduced by the assimilation process, as highlighted by the AN departures (red lines) being closer to zero than the BG departures (green lines). Note that the difference between the BG and the AN departure is equal to the analysis increments associated with the related observations (i.e. AN–BG).

The number of observations assimilated is different for each satellite instrument and varies with time. IASI generates the largest number of data, with both instruments (IASI-A and IASI-B) providing between 150 000 and 200 000 XCO<sub>2</sub> or XCH<sub>4</sub> data per month. The observations taken by SCIAMACHY oscillate between 25 000 and 50 000 data per month for CH<sub>4</sub> and between 5000 and 10 000 data per month for CO<sub>2</sub>. The number of GOSAT XCO<sub>2</sub> data fluctuates around 2500, whereas GOSAT XCH<sub>4</sub> measurements are comprised of between 5000 and 10 000 data per month. It is also clear

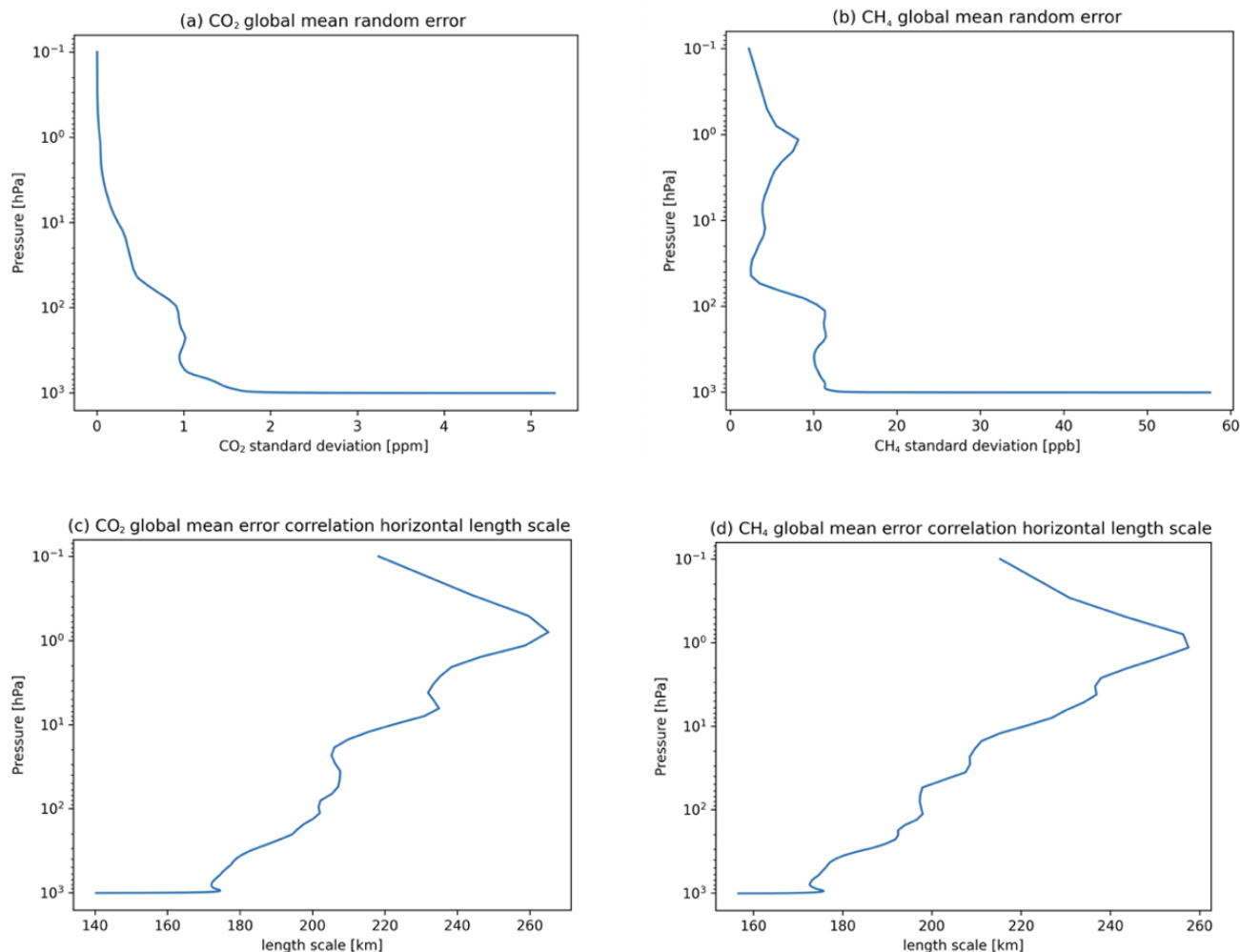


**Figure 4.** Model background error for CO<sub>2</sub> and CH<sub>4</sub> used in the CAMS GHG reanalysis: (a, b) global mean standard deviation and (c, d) global mean error correlation length scale across the vertical levels.

from Figs. 5a, d and 6a, d that fewer XCO<sub>2</sub> and XCH<sub>4</sub> data from SCIAMACHY, IASI and GOSAT-TANSO are assimilated during the winter months. A vertical dashed magenta line in Figs. 5c, d and 6c, d indicates when the near-real-time satellite products started to be assimilated in early 2019. This transition produced an abrupt change in the quality and availability of both IASI and GOSAT retrievals.

The modelled XCO<sub>2</sub> is systematically larger than the observations (leading to overall negative BG departures) because of the biases in the total fluxes (see Sect. 2.3). Therefore, all instruments produced negative departures until 2013 (Fig. 5). From 2013 to 2019, the modelled values of XCO<sub>2</sub> became smaller than those measured by GOSAT (Fig. 5d), while the model continued to (slightly) overestimate the IASI XCO<sub>2</sub> observations in the middle to upper troposphere. This overestimation is consistent with a drift in the IASI CO<sub>2</sub> data towards a growing negative bias. After 2018, part of the drift is due to the fact that IASI (version v4.0) is saturated with

increasing atmospheric CO<sub>2</sub>. Note that this has been corrected with v9.1 (available on the C3S data store). A sudden change in the IASI-B XCO<sub>2</sub> departures is visible in Fig. 5c around December 2018, corresponding to the switch from the ESA-CCI reprocessed dataset to a near-real-time LMD dataset used operationally in the CAMS GHG analysis. The transition to a new dataset was made necessary as the reanalysis production was running close to real time and reprocessed observations were not available. After the transition to near-real-time observations, the IASI XCO<sub>2</sub> increments are reduced to almost zero, as hinted to by the overlap between the red (AN departure) and green lines (BG departure) in Fig. 5c. At the same time, a drop in the number of assimilated IASI XCO<sub>2</sub> observations is observed (blue line, Fig. 5c). Together with a drastic reduction in the magnitude of the increments, a large negative bias of approximately 5 ppm in both the AN and BG departures emerges. This degradation in the quality of the IASI-B XCO<sub>2</sub> observations in the near-

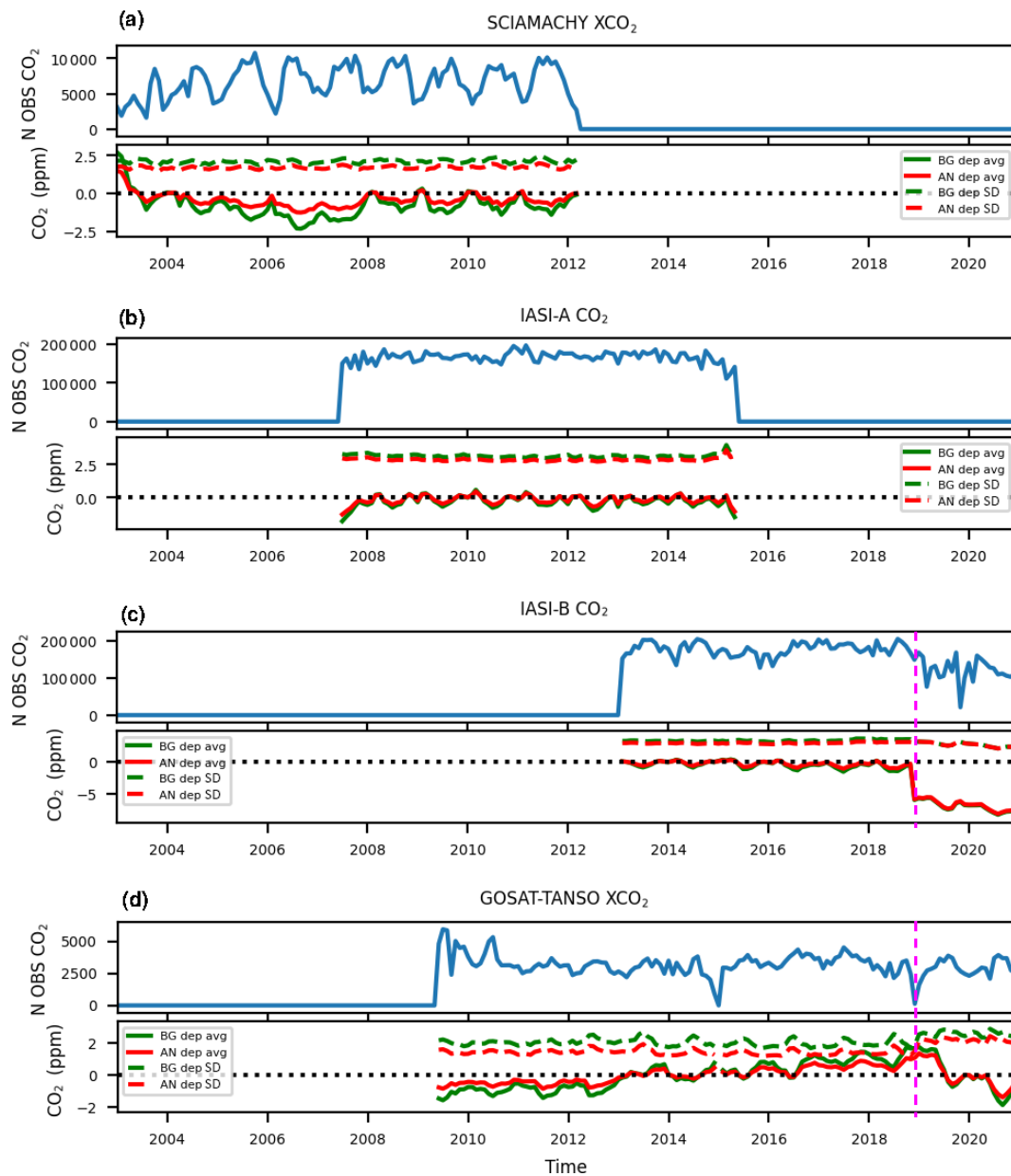


**Figure 5.** Time series of the global monthly number of XCO<sub>2</sub> satellite data (blue) and monthly mean CO<sub>2</sub> analysis (AN) and model background (BG) departures of the various observations (OBS) assimilated in the reanalysis (AN-OBS and BG-OBS in red and green, respectively; see the legend). The solid lines show the monthly average of the departures, and the dashed lines show the monthly standard deviations. The dashed magenta line indicates the switch to the near-real-time satellite products. Note that the range of values on the y axis varies depending on the satellite product.

real-time dataset is due to the change in the correction of the non-linearity of the detector of IASI-B that was made by CNES and EUMETSAT on 17 August 2018 that introduced a bias of  $\sim 0.2$  K into the channels used to perform the CO<sub>2</sub> retrieval. This change has been corrected in the versions of IASI-B MT-CO<sub>2</sub> that are available on the C3S data store, but these versions were not used for this reanalysis. In January 2019, there was also a transition from the ESA-CCI GOSAT XCO<sub>2</sub> retrievals to the near-real-time IUP-UB retrieval prod-

uct (Heymann et al., 2015; Massart et al., 2016), as shown in Fig. 5d. Consequently, the standard deviation of both the AN and the BG departures increases (dashed lines, Fig. 5d), suggesting that the near-real-time data are noisier than the reprocessed dataset from ESA-CCI.

The mean XCH<sub>4</sub> departures (both AN and BG) of SCIAMACHY and IASI are relatively small (a few ppb) compared to GOSAT (up to 10 ppb) throughout the entire time period (see the solid red and green lines in Fig. 6). The XCH<sub>4</sub> SCIA-

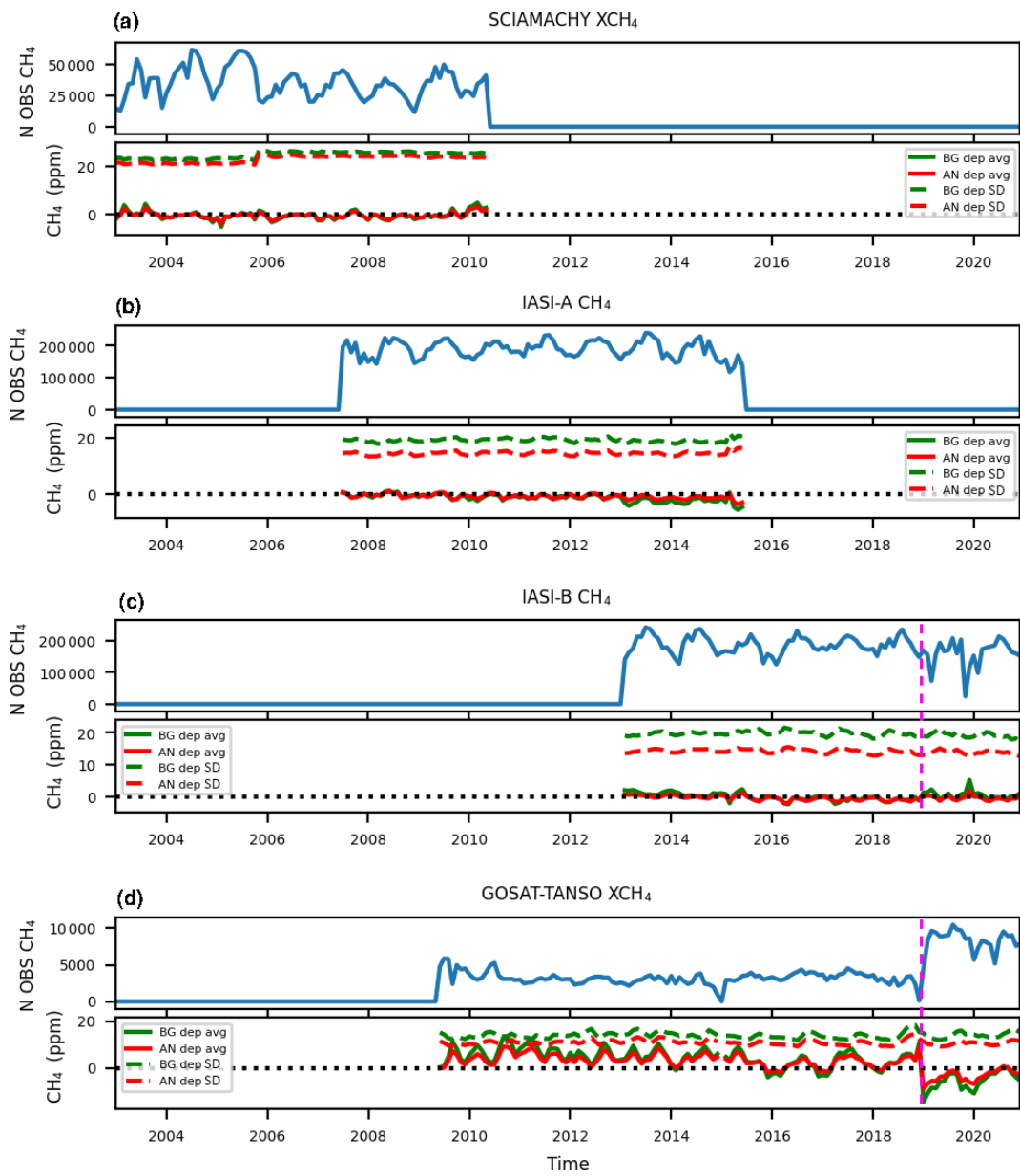


**Figure 6.** Time series of the global monthly number of XCH<sub>4</sub> satellite data (blue) and monthly mean CH<sub>4</sub> analysis (AN) and model background (BG) departures of the various observations (OBS) assimilated in the reanalysis (AN-OBS and BG-OBS in red and green, respectively; see the legend) for different satellite products. The solid lines show the monthly average of the departures, and the dashed lines show the monthly standard deviations. The dashed magenta line indicates the switch to the near-real-time satellite products. Note that the range of values on the y axis varies depending on the satellite product.

MACHY data were not used from 9 April 2012 onwards (Fig. 6a). The standard deviation of both the AN and BG departures are smaller for GOSAT (around 10 ppb, dashed lines in Fig. 6d) than for SCIAMACHY (around 20 ppb, dashed lines in Fig. 6a), indicating that GOSAT provides less noisy observations. Similar to what was observed for CO<sub>2</sub>, a discontinuity in the mean AN and BG departures of GOSAT XCH<sub>4</sub> emerges in January 2019, corresponding to transition from the ESA-CCI dataset and the NRT SRON retrievals

(see the dashed magenta line in Fig. 6d). Both the AN and the BG departures change sign, indicating that while up to 2019 both the analysis and model were underestimating the GOSAT observations, they started to overestimate them after 2019. Since there was no modification to the model used for the reanalysis over this period, the cause of this negative bias emerging in both the AN and the BG departures since 2019 can only be attributed to the NRT GOSAT XCH<sub>4</sub> observations, and in particular to the fact that they are generated

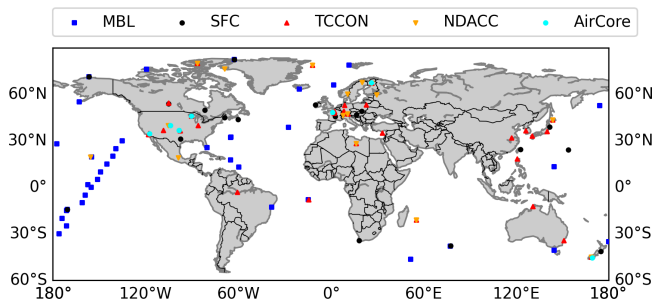


**Figure 7.** Map with observation sites used in the evaluation of the CAMS GHG reanalysis: the marine boundary layer (MBL, blue squares) includes NOAA MBL reference sites used to compute the NOAA global mean CO<sub>2</sub> and CH<sub>4</sub> mole fraction product (see <https://gml.noaa.gov/ccgg/mbl/mbl.html>, last access: 18 March 2023, for further details), SFC (black circles) corresponds to the in situ near-surface continuous observations of CO<sub>2</sub> and CH<sub>4</sub>, TCCON and NDACC sites are depicted by red and orange triangles, and AirCore sites are shown by cyan circles.

by using an extrapolated XCO<sub>2</sub> value in the proxy retrieval. In addition, the number of assimilated NRT GOSAT XCH<sub>4</sub> observations approximately doubles (blue line in Fig. 6d). Note that the switch to the near-real-time retrievals for IASI-B XCH<sub>4</sub> has a much more marginal impact on the system (Fig. 6c).

### 3 Evaluation with independent observations

Validation against a set of independent observations has been performed on the 18 years of the CAMS GHG reanalysis span. The independent data include different types of observations (see Fig. 7): in situ near-surface continuous observations of CO<sub>2</sub> and CH<sub>4</sub> mole fractions from the collaborative ObsPack datasets (Masarie et al., 2014; Schuldt et al., 2020, 2021; NOAA Carbon Cycle Group ObsPack Team, 2019; see Table A1), dry-air column-averaged mole fractions from the Total Carbon Column Observing Network (TCCON; Wunch et al., 2011, 2015), tropospheric and stratospheric partial columns for CH<sub>4</sub> from the Network for the Detection of Atmospheric Composition Change (NDACC; De Mazière et al., 2018) (see Table A2), AirCore vertical profiles of CO<sub>2</sub> and CH<sub>4</sub> mole fractions (Karion et al., 2010; Baier et al., 2021), and the NOAA global mean CO<sub>2</sub> and CH<sub>4</sub> mole fraction product based on the Greenhouse Gas Marine Boundary Layer Reference (Conway et al., 1994; Dlugokencky et al., 1994; Masarie and Tans, 1995).

#### 3.1 Surface and column data

##### 3.1.1 Carbon dioxide

Overall, the error is within  $\pm 10$  and  $\pm 4$  ppm for most of the near-surface and total column stations, respectively, for the whole 18-year period (Figs. 8 and 9). Near the surface

(Fig. 8), there is a large variability in the CO<sub>2</sub> error between continental stations influenced by local fluxes (e.g. CDL, FSD, AMT, HUN; see Table A1) and oceanic stations sampling well-mixed air (e.g. ALT, BRW, MHD). Continental stations show large error variations with season (e.g. CDL, HUN) and show an underestimation of CO<sub>2</sub> in the summer and an overestimation in the winter, indicating an underestimation of the amplitude of the CO<sub>2</sub> seasonal cycle largely driven by vegetation growth. Differences between stations will be determined by the footprint of observations having different contributions of fluxes from different biomes and from anthropogenic emissions. The accuracy of such fluxes can vary geographically.

Overall, there is positive bias of a few parts per million between 2003 and 2015 in the baseline surface stations (e.g. BRW, SMO, SPO), which is consistent with the XCO<sub>2</sub> error at the TCCON sites (Fig. 9). This positive bias decreases from 2007 to 2015 when IASI-A CO<sub>2</sub> data are assimilated, with values lower than 2 ppm, and becomes negative from 2015 to 2019 (from 0 to  $-2$  ppm). From 2019 onwards, there is a positive trend in the bias, and it becomes positive ( $> +2$  ppm) in 2020. There is consistency between the column and surface biases, with a general positive bias at background stations before 2015 and a negative bias after 2015 (up to 2019) at the surface stations, although there are no data in 2020 from the surface stations.

The synoptic and large-scale variability of CO<sub>2</sub> is well represented by the reanalysis (Fig. 9b). The root-mean-square error at TCCON stations is below 0.8 ppm for XCO<sub>2</sub>. The normalised standard deviation is around 1.0 ( $\pm 0.3$ ), and the Pearson correlation coefficient is larger than 0.8.

##### 3.1.2 Methane

The CH<sub>4</sub> reanalysis fields are generally in good agreement with surface and tropospheric column observations, with typical weekly and monthly errors within  $\pm 40$  and  $\pm 25$  ppb, respectively (Figs. 10, 11 and 12). Stratospheric partial columns compared to the NDACC data reveal a positive bias that is of the same order as the reported measurement uncertainty of 7 % (Fig. 10a). The averaged relative differences in the troposphere across all NDACC sites are  $-0.4$  % for the reanalysis (Fig. 11b), which is well within the measurement's uncertainty. The reanalysis overestimates the column-averaged CH<sub>4</sub> compared to TCCON observations (Fig. 12) for most mid- and high-latitude sites, with a relative difference of up to 2.5 %, but shows a good agreement for the low-latitude sites at Izaña, Darwin and Wollongong. At the surface the bias is overall positive up to 2007 (Fig. 10). With the introduction of IASI, the biases are reduced. However, with the switch to near-real-time satellite data, the bias become negative at all sites, reaching values lower than  $-20$  ppb.

Differences between the surface and total column biases stem from the fact that the model suffers from large positive biases above the tropopause (between 100 and 10 hPa)

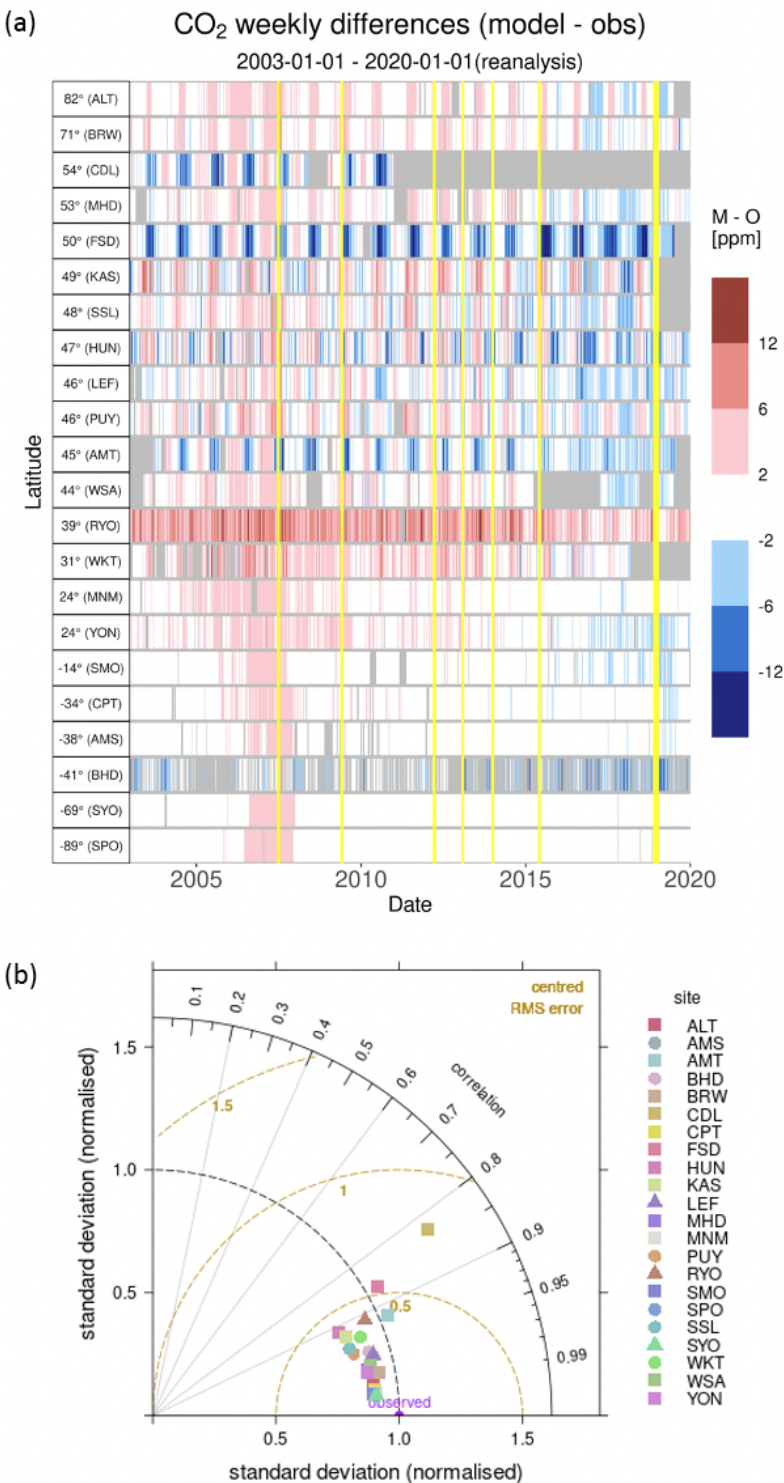


**Figure 8.** (a) Mosaic plot of CO<sub>2</sub> weekly biases (in ppm) of the CAMS GHG reanalysis compared to surface continuous observations of CO<sub>2</sub> mole fraction obtained from the GLOBALVIEWplus CO<sub>2</sub> ObsPack v6.0 (Schuldt et al., 2020) listed in Table A1. Each coloured vertical line represents a weekly mean. Vertical yellow lines depict the changes in the assimilated data documented in Figs. 1, 5 and 6. Grey shading indicates no observations are available. (b) Taylor diagrams for the site-dependent CO<sub>2</sub> comparison of the CAMS GHG reanalysis against the same observations used in (a). The standard deviation is normalised by dividing the observed and modelled time series by the standard deviation of the observations. The model has higher (lower) variability compared to the observed data if the site is plotted with a distance (smaller) than 1 from the origin.

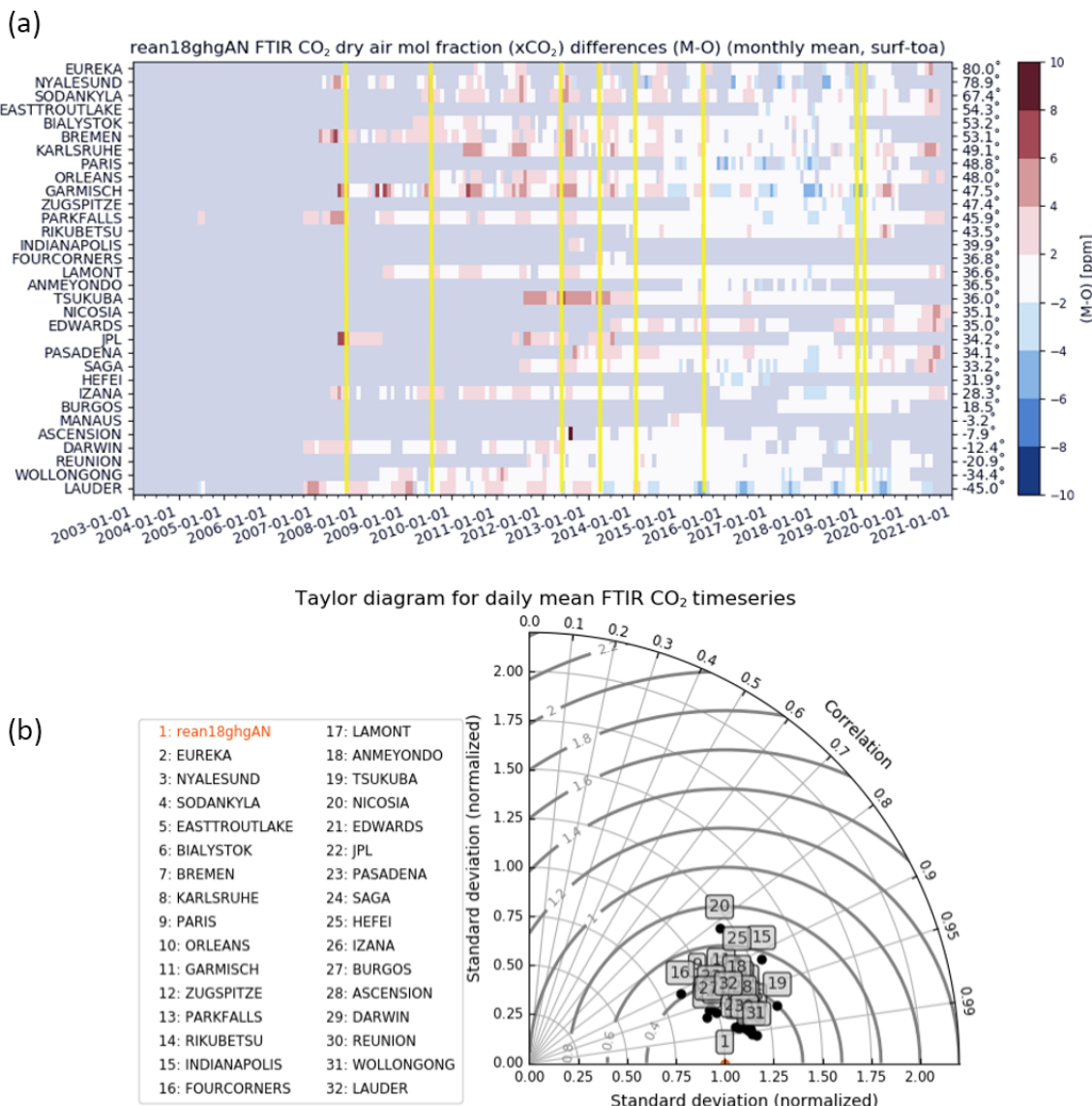


**Figure 9.** (a) Mosaic plot of the CAMS GHG reanalysis biases at all TCCON sites (see Table A2) for the column-averaged dry mole fraction of CO<sub>2</sub> (ppm) (XCO<sub>2</sub>) averaged daily around local noon ( $\pm 2.5$  h). Vertical yellow lines depict the changes in the assimilated data documented in Figs. 1, 5 and 6. Grey shading indicates no observations are available. (b) Taylor diagrams for the station-dependent XCO<sub>2</sub> comparison of the CAMS GHG reanalysis against TCCON Fourier transform infrared (FTIR) data. The standard deviation is normalised by dividing the observed and modelled time series by the standard deviation of the model time series. The model has higher (lower) variability compared to the observed data if the site is plotted with a distance smaller (larger) than 1 from the origin.

of about 80–100 ppb during the months between September and November (Figs. 5d and 6d of Verma et al., 2017) that affect the total column average. This stratospheric bias cannot be corrected systematically by CH<sub>4</sub> satellite data from SCIAMACHY, GOSAT and IASI.

For all observations (surface, partial and total columns) CH<sub>4</sub> shows a seasonality in the relative difference between observations and the reanalysis. The magnitude of the difference is site dependent. During local autumn and winter months the relative bias is increased (underestimation) at most surface sites and in the tropospheric columns. This

underestimation is also seen in the TCCON time series. In spring and summer there is an overestimation of CH<sub>4</sub> near the surface and in the total column. These biases are related to errors in the seasonal cycle of surface emissions, most likely from agriculture and wetlands, and the accuracy of the representation of the hydroxyl radical (OH) sink, which overall have larger values in the climatology compared to CAMS IFS (CB05-BASCOE) atmospheric chemistry model OH (Segers et al., 2020b; Williams et al., 2022). The XCH<sub>4</sub> root-mean-square error is around 1.4 ppb, and the Pearson correlation coefficient is larger than 0.7 for XCH<sub>4</sub> except for some out-

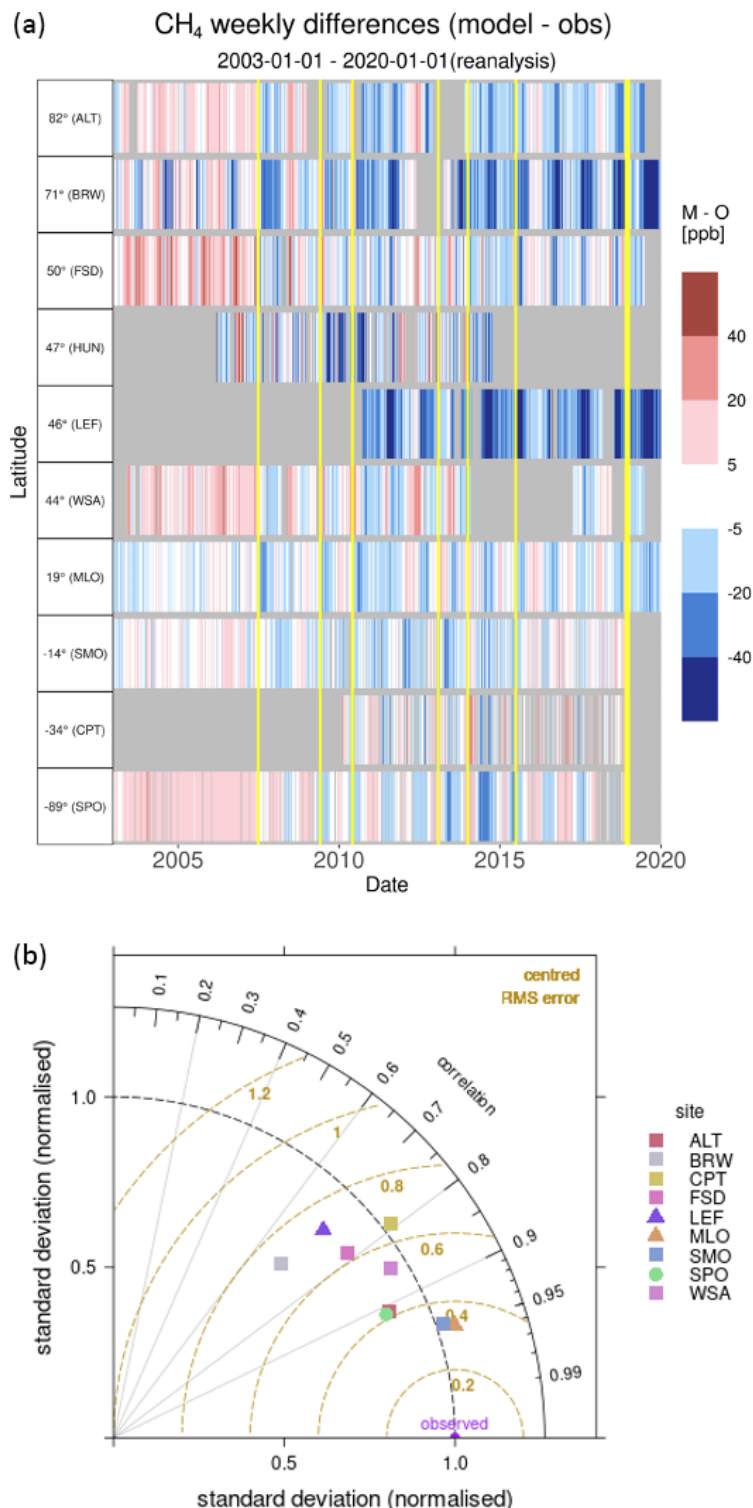


**Figure 10.** (a) Mosaic plot of CH<sub>4</sub> biases (in ppb) compared to surface continuous observations from GLOBALVIEWplus CH<sub>4</sub> ObsPack v1.0 data product (Cooperative Global Atmospheric Data Integration Project, 2019) listed in Table A1. Each coloured vertical line represents a weekly mean. Vertical yellow lines depict the changes in the assimilated data documented in Figs. 1, 5 and 6. Grey shading indicates no observations are available. (b) Taylor diagrams for the site-dependent CH<sub>4</sub> comparison of the CAMS GHG reanalysis against same as the observations used in (a). The standard deviation is normalised by dividing the observed and modelled time series with the standard deviation of the observations. The model has higher (lower) variability compared to the observed data if the site is plotted with a distance larger (smaller) than 1 from the origin.

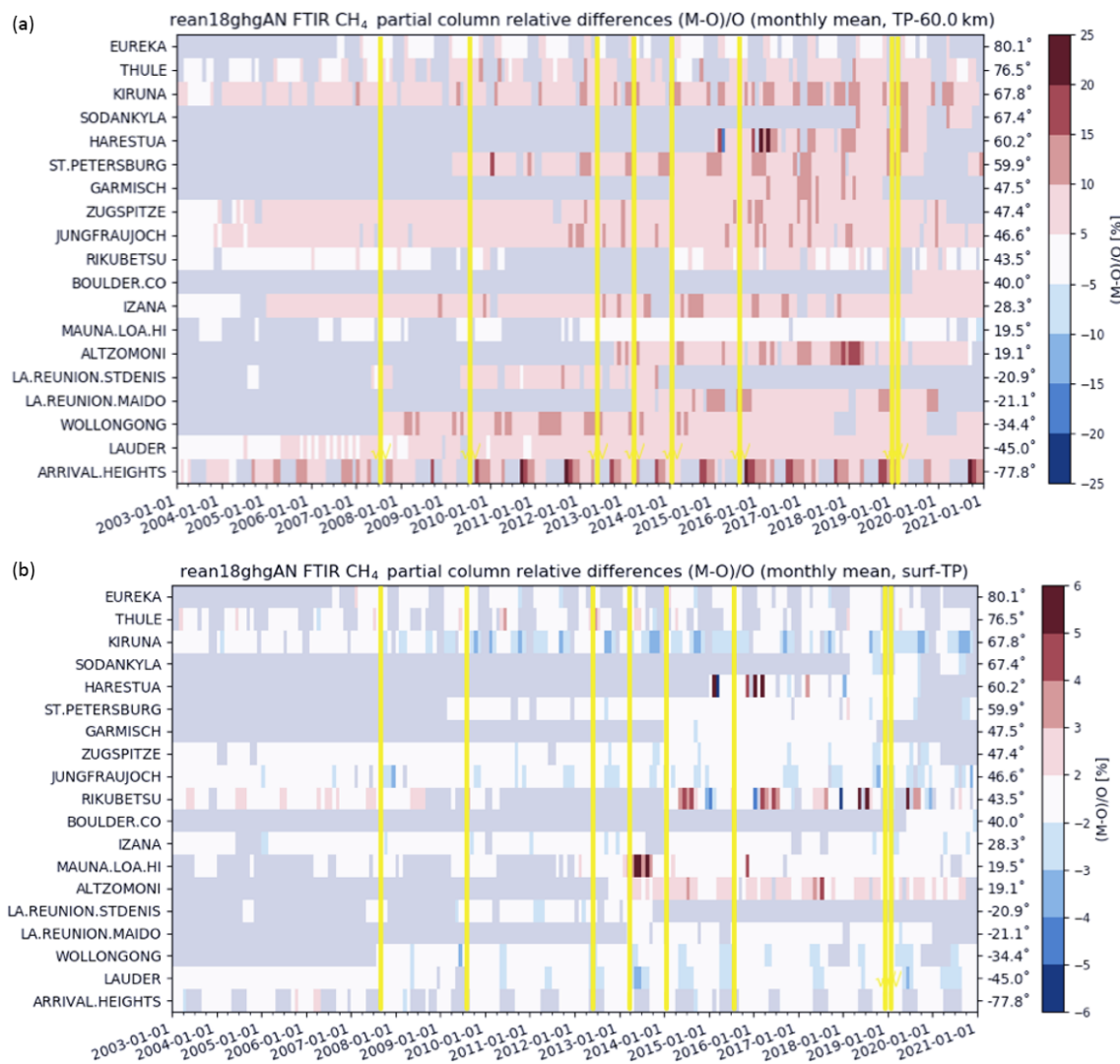


**Figure 11.** Mosaic plot of seasonal relative  $\text{CH}_4$  biases at all FTIR sites (see Table A2) for the stratospheric columns (a) and tropospheric columns (b) from NDACC. Vertical yellow lines depict the changes in the assimilated data documented in Figs. 1, 5 and 6. Grey shading indicates no observations are available.

liers (Fig. 12b), indicating a good representation of the synoptic variability (as for  $\text{XCO}_2$ ).

### 3.2 Vertical profiles

The uncertainty in the CAMS GHG reanalysis varies with height, and the accuracy of the analysis vertical profiles depends mostly on the underlying model uncertainty, as the satellite data assimilated in the reanalysis only provide integrated total or partial atmospheric columns. The reanalysis has been evaluated using observations of  $\text{CO}_2$  and  $\text{CH}_4$  vertical profiles (Karion et al., 2010; Baier et al., 2021) from the NOAA AirCore dataset v20210813. It includes 133 vertical profiles from the surface to the lower stratosphere (up to around 40 hPa) from 2012 to 2020 at the seven sites listed in Table A3.

Figure 13 shows that the largest mean errors occur (i) near the surface with a strong influence from surface fluxes, (ii) in the upper troposphere–lower stratosphere (UTLS) region (between 500 and 100 hPa) with a strong influence from long-range transport, (iii) in the stratosphere (above 100 hPa) where uncertainties associated with chemical loss of  $\text{CH}_4$  and the meteorology driving the tracer transport are largest, and the fact that satellite data used here are not able to constrain the stratospheric  $\text{CO}_2$  and  $\text{CH}_4$  in the reanalysis. Near the surface, there is a positive  $\text{CO}_2$  bias associated with an overestimation of the total flux in the model and a negative  $\text{CH}_4$  bias that stems from both errors in the emissions and the chemical loss rate in the troposphere. The negative  $\text{CO}_2$  bias in the UTLS agrees with the tendency of the model to underestimate fine-scale higher-valued  $\text{CO}_2$  streamers associated with long-range transport. The large positive  $\text{CH}_4$  bias

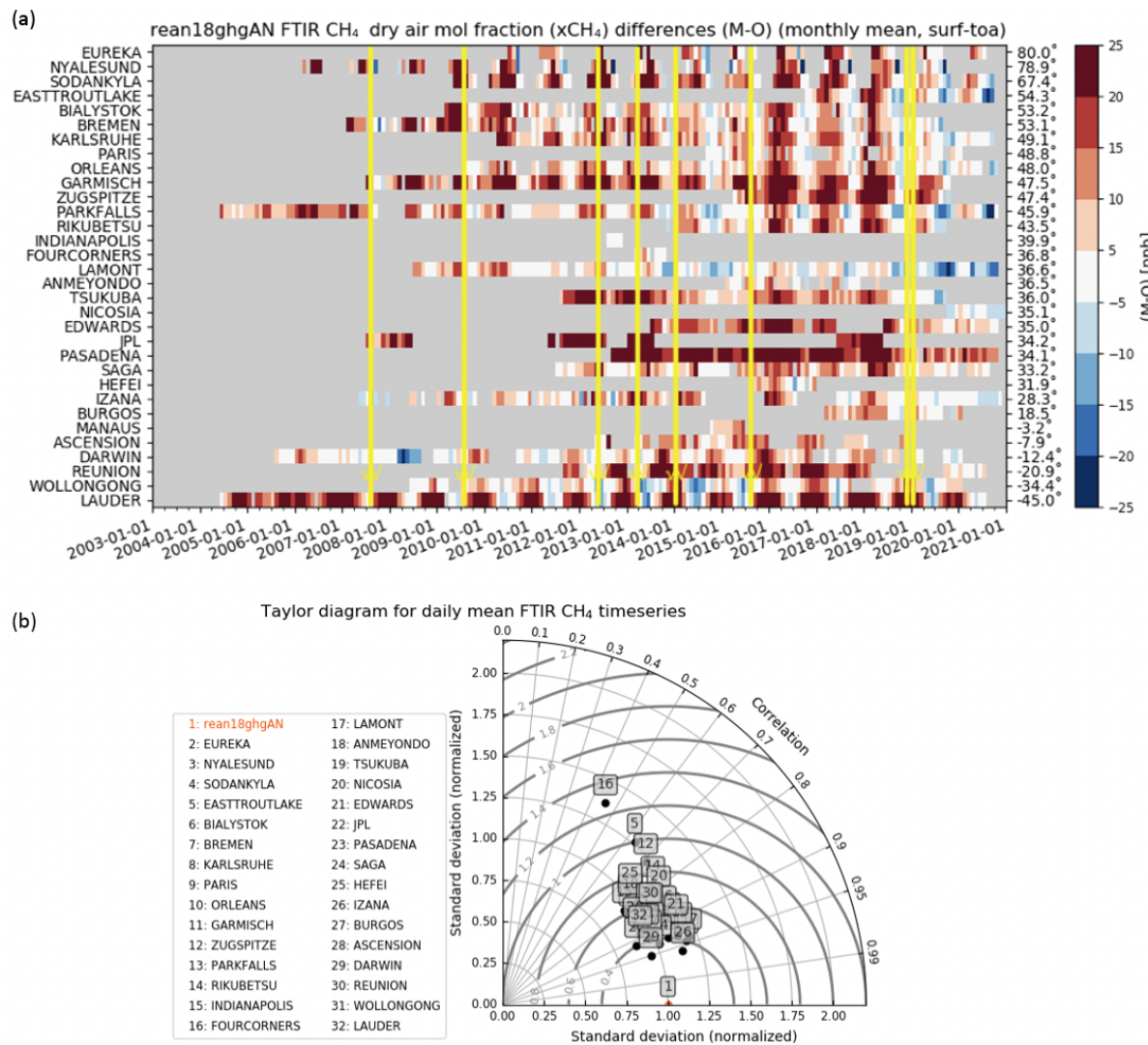


**Figure 12.** (a) Mosaic plot of monthly biases at all TCCON sites for the column-averaged mole fractions  $\text{XCH}_4$  (ppb) averaged daily around local noon ( $\pm 2.5$  h). Vertical yellow lines depict the changes in the assimilated data documented in Figs. 1, 5 and 6. Grey shading indicates no observations are available. (b) Taylor diagrams for the station-dependent  $\text{XCH}_4$  comparison of the CAMS GHG reanalysis against TCCON FTIR data. The standard deviation is normalised by dividing the observed and modelled time series by the standard deviation of the model time series. The model has higher (lower) variability compared to the observed data if the site is plotted with a distance smaller (larger) than 1 from the origin.

in the stratosphere of around 200 ppb is consistent with the positive biases with respect to NDACC stratospheric column (Fig. 11a) and the documented model biases with respect to MIPAS and ACE-FTS by Verma et al. (2017). The errors associated with the stratospheric chemical sink are thought to be the largest contributor to the stratospheric  $\text{CH}_4$  bias, as shown by tests using the IFS CB05-BASCOE chemical loss rate (not shown here). In general, the reanalysis underestimates the  $\text{CO}_2$  vertical gradient across the tropopause. This underestimation leads to a positive bias for  $\text{CO}_2$  in the lower stratosphere of around 2 ppm. The analysis is not able to remove the large errors near the surface by only adjusting the

atmospheric mole fractions, i.e. without adjusting the emissions in the data assimilation process, nor it is able to reduce the stratospheric errors in the model (Massart et al., 2017; Verma et al., 2017). The vertical profiles have a large variability from day to day, as shown in Fig. 14 with a sequence of profiles at Traînou (France). The CAMS GHG reanalysis is able to capture these synoptic variations in the vertical profile, consistent with its skill in representing  $\text{XCO}_2$  and  $\text{XCH}_4$  synoptic variability (Figs. 9b and 12b). For a full catalogue of all the individual AirCore vertical profiles used in Fig. 13, see the Supplement.

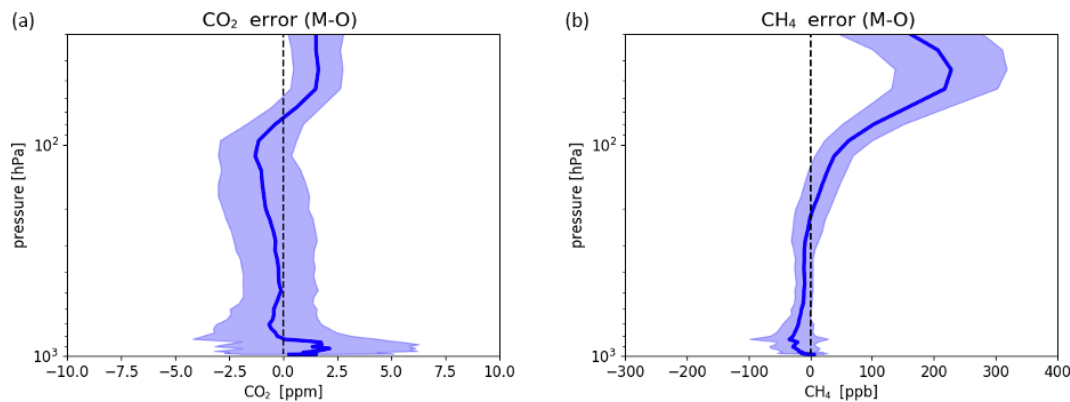


**Figure 13.** Vertical profiles of mean error (model minus observation, M–O) of CAMS CO<sub>2</sub> (a) and CH<sub>4</sub> (b) reanalysis with respect to AirCore observations comprising 133 profiles at seven sites (listed in Table A3) over the period from 2012 and 2020. The blue shading shows the  $\pm$  standard deviation of M–O with respect to the mean error. The vertical dashed black line depicts the zero mean error.

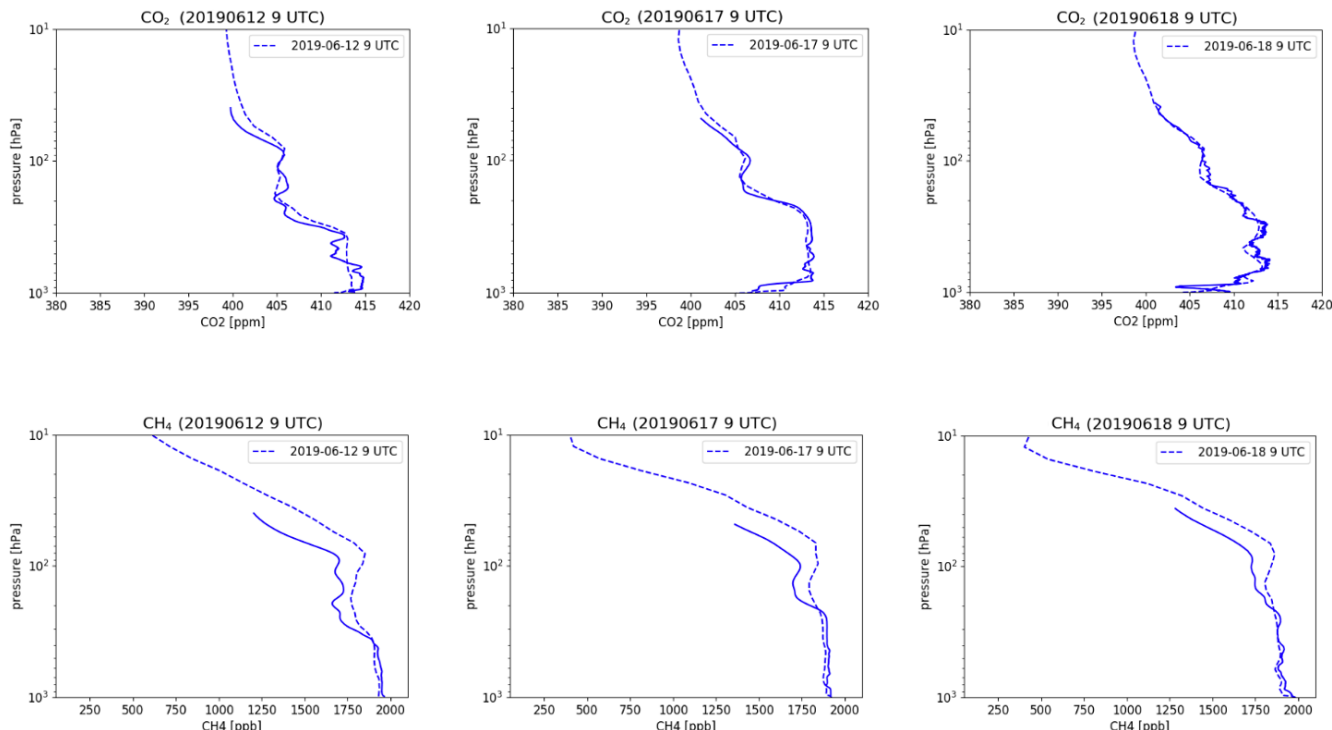


**Figure 14.** Vertical mole fraction profiles of CO<sub>2</sub> and CH<sub>4</sub> from the CAMS GHG reanalysis (dashed line) and AirCore observations (solid line) at Trafnou (France; see Table A3) over the period in June 2019.

### 3.3 Trends

Although this reanalysis uses a consistent underlying model and reprocessed observations of CO<sub>2</sub> and CH<sub>4</sub>, the current system is not able to provide an accurate enough atmospheric mole fraction for use in estimating trends and atmospheric growth rates as computed by the changes in global mean CO<sub>2</sub> and CH<sub>4</sub> from 1 year to the next. The CO<sub>2</sub> and CH<sub>4</sub> global annual means based on marine boundary layer (MBL) reference sites are compared to the NOAA Global

Greenhouse Gas Reference Network (GGGRN) observations (<https://gml.noaa.gov/ccgg/about.html>, last access: 18 March 2023; Andrews et al., 2014; Conway et al., 1994; Dlugokencky et al., 1994) in Fig. 15. Changes in the assimilated satellite data have a clear impact on the evolution of the global annual mean values of CO<sub>2</sub> and CH<sub>4</sub> in the CAMS GHG reanalysis. The reanalysis has a positive global bias in near-surface CO<sub>2</sub> and CH<sub>4</sub> of a few parts per million and around 20 ppb, respectively, from 2003 to 2007. Note that this positive bias in the annual global mean does not imply

that the bias will be positive everywhere, as shown by the negative surface CH<sub>4</sub> biases at the AirCore sites (Fig. 13) and the large temporal and geographical variability in the weekly bias illustrated in Figs. 8 and 10. After the introduction of IASI in 2007 the global bias decreases and is at its lowest during the period when the number of observations is largest in 2013 and 2014 (Figs. 5 and 6). Finally, the change to the near-real-time satellite retrievals in 2019 and the incorrect trend in the emissions during the COVID-related slowdown period in 2020 (Le Quéré et al., 2020) lead to changes in the global bias from negative to positive for CO<sub>2</sub> and from positive to negative for CH<sub>4</sub>. These changes in the global bias are consistent with the changes in the errors with respect to total column and near-surface observations in Figs. 8 to 12. It is important to note that the changes in global bias associated with changes in the assimilated data are of the same order of magnitude as the observed atmospheric growth rates of CO<sub>2</sub> (<https://gml.noaa.gov/ccgg/trends>, last access: 18 March 2023) and CH<sub>4</sub> ([https://gml.noaa.gov/ccgg/trends\\_ch4](https://gml.noaa.gov/ccgg/trends_ch4), last access: 18 March 2023). For this reason, this reanalysis product is not suitable for trend analysis.

#### 4 Limitations and caveats

This section provides an overview of the shortcomings of the CAMS GHG reanalysis that users should consider when interpreting the data. The main issues documented in the previous sections are summarised below.

1. Emissions are prescribed and not adjusted by the data assimilation system in the CAMS reanalysis (Sect. 2.3). This leads to a growing model error for CO<sub>2</sub> and CH<sub>4</sub> that can be difficult to correct with a sparse observing system and 12 h assimilation window. In addition, the prescribed emissions are not available as near-real-time data, which means they are either kept fixed since the last year available (e.g. 2010 for CH<sub>4</sub>) or extrapolated with a climatological trend as was done for CO<sub>2</sub> (see details in Sect. 2.3). Because of this, the CAMS GHG reanalysis is not suitable to investigate the impact of local emission changes, such as COVID impact studies, which require a large local emission adjustment to the prescribed inventories (e.g. Doumia et al., 2021) and atmospheric inversion systems to estimate the changes (e.g. McNorton et al., 2022).
2. Changes in satellite data used with different temporal, horizontal and vertical coverage cause changes in the quality of the reanalysis. For example, winter seasons have a lower number of observations because of light conditions and the higher frequency of cloud presence. This affects the quality of the seasonal cycle and the inter-hemispheric gradient. Similarly, in regions where there is no observation coverage, such as the stratosphere, the reanalysis is based on the underlying model

including its systematic errors (see the discussion of stratospheric biases in Sect. 3.2).

3. Changes in satellite retrievals affect the quality of the observations used in the CAMS GHG reanalysis. For example, the switch from the CCI reprocessed satellite products to the near-real-time products is associated with a marked change in the bias and random error (i.e. standard deviation) of the departures from XCO<sub>2</sub> and XCH<sub>4</sub> GOSAT observations and in the bias of the departures from the XCO<sub>2</sub> IASI-B observations. This large increase in the bias of the assimilated CO<sub>2</sub> and CH<sub>4</sub> observations from 2019 onwards results in a large increase in the bias of the CAMS GHG reanalysis in 2019 and 2020, which has implications for the trend analysis (Sect. 3.3).
4. The fixed climatological chemical loss rate of CH<sub>4</sub> (Sect. 2.3) has been shown to overestimate the atmospheric CH<sub>4</sub> chemical sink by Segers et al. (2020b). Preliminary tests coupling the IFS to the atmospheric loss rate derived from CB05-BASCOE chemistry have indeed shown a large reduction in the CH<sub>4</sub> negative bias at mid-latitudes. Systematic errors in the CH<sub>4</sub> chemical sink used in this reanalysis may have contributed further to enhancing the large negative CH<sub>4</sub> bias in the CAMS GHG reanalysis over the last period in 2020, when the increase in the CH<sub>4</sub> growth rate is linked to a decrease in chemical loss rate (Stevenson et al., 2022).
5. The large CH<sub>4</sub> and CO<sub>2</sub> biases in the stratosphere are currently under investigation. The CH<sub>4</sub> stratospheric bias is mainly associated with the use of a climatological loss rate (Sect. 2.3), as preliminary tests using a different chemical loss rate based on IFS CB05-BASCOE simulations show that the bias in CH<sub>4</sub> is greatly reduced.
6. Changes in systematic errors with time due to model error and changes in observation coverage and quality will affect trend analysis (see Sect. 3.3).

An up-to-date list of the known issues of the CAMS reanalysis can be found on the online CAMS documentation website (<https://confluence.ecmwf.int/display/CKB/CAMS%3A+Reanalysis+data+documentation>, last access: 18 March 2023). Some of these issues will also be addressed in the future CAMS reanalysis (planned to start production in 2024), including the improvement of the prescribed emission trends, the consistent use of satellite retrieval products and the use of a variable CH<sub>4</sub> chemical loss rate.

#### 5 Summary and conclusions

This technical report documents the first CAMS IFS reanalysis of CO<sub>2</sub> and CH<sub>4</sub> produced by ECMWF that complements

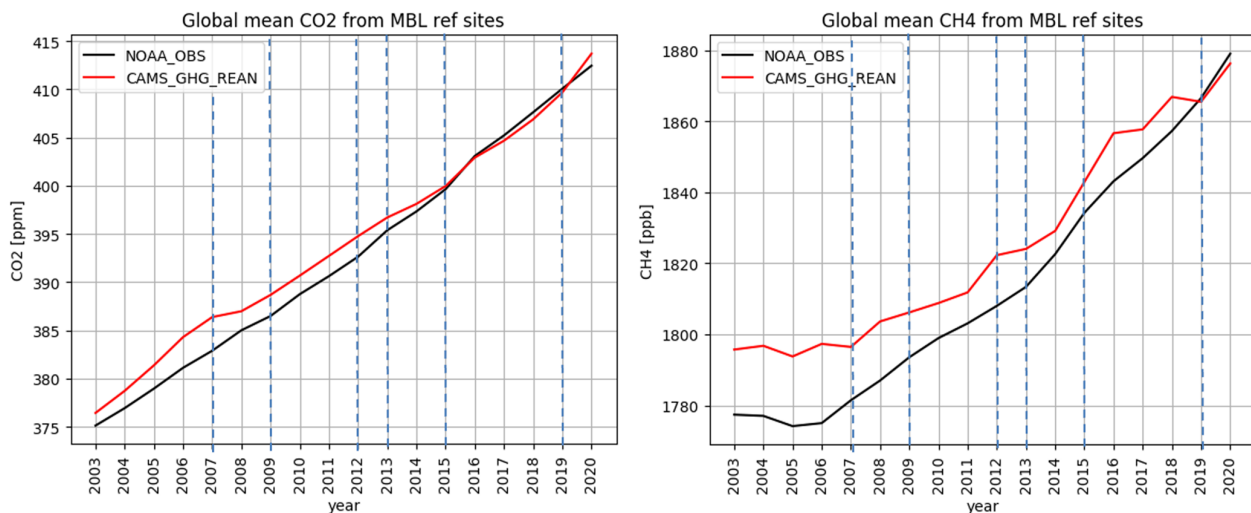


**Figure 15.** Global mean CO<sub>2</sub> (ppm) and CH<sub>4</sub> (ppb) from the CAMS GHG reanalysis (in red) and the NOAA global mean CO<sub>2</sub> and CH<sub>4</sub> (in black, <https://gml.noaa.gov/ccgg/trends/global.html>, last access: 18 March 2023) based on the Greenhouse Gas Marine Boundary Layer Reference (Conway et al., 1994; Dlugokencky et al., 1994, 2021; Masarie and Tans, 1995). The global mean of the CAMS GHG reanalysis has been computed based on the same NOAA marine boundary layer (MBL) reference sites shown in Fig. 7 (see <https://gml.noaa.gov/ccgg/mbl/mbl.html> for further details). The dashed blue lines mark the years when there was a change in the observing system. The uncertainty associated with the computation of global mean using the MBL sites is estimated to be 0.1 ppm for CO<sub>2</sub> (Ed Dlugokencky and Pieter Tans, NOAA/GML, <https://gml.noaa.gov/ccgg/trends>) and below 2 ppb for CH<sub>4</sub> (Ed Dlugokencky, NOAA/GML; [https://gml.noaa.gov/ccgg/trends\\_ch4](https://gml.noaa.gov/ccgg/trends_ch4)).

the CAMS reanalysis of reactive gases and aerosols (Inness et al., 2019). The processing chain, assimilated satellite data and underlying model used are described, and the resulting reanalysis is evaluated using independent in situ near-surface observations, total column retrievals and in situ atmospheric profile observations. The monthly systematic and random errors of CO<sub>2</sub> and CH<sub>4</sub> typically range within 1 % from 2003 to 2020 with an overall good skill in the representation of synoptic spatial variability and seasonal cycle. The lowest systematic errors occur in the period with the maximum number of observations in 2013 and 2014. In 2019 there was a switch from C3S pre-processed satellite products to the near-real-time CAMS satellite products because at the time of production the C3S products had not reached 2019. This caused a jump in the quality of the satellite data and the resulting CAMS GHG reanalysis. For this reason, a new rerun of the CAMS GHG reanalysis from 2019 onwards will be performed with consistent C3S satellite products in the near future.

The comparison of global mean values with observations shows variations in the bias that depend on changes in the assimilated satellite data of around 2 ppm and 10 ppb for CO<sub>2</sub> and CH<sub>4</sub>, respectively, which have the same magnitude as the observed variations in their growth rate. For this reason, we do not recommend the use of this dataset to study changes in the atmospheric growth rate of CO<sub>2</sub> and CH<sub>4</sub>. Similarly, large biases in stratospheric CO<sub>2</sub> and CH<sub>4</sub> should also be considered when analysing stratospheric signals and trends

in the CAMS GHG reanalyses. A list of caveats and limitations that users need to be aware of is provided in Sect. 4.

The slow reduction in the lingering bias in the model background is associated with the following competing factors at play: (i) the error growth in the model background associated with the accumulation of systematic errors in emission and natural fluxes, (ii) the limited coverage of observations in time and space (both horizontal and vertical), and (iii) the localised impact of observations associated with a short data assimilation window spanning 12 h.

In order to improve the CAMS reanalysis in future releases we recommend the following actions: (i) increase the number and coverage of satellite data assimilated from additional satellite missions such as the Copernicus Sentinel-5 Precursor (S5P), Orbiting Carbon Observatory 2 and 3 (OCO-2, [https://www.nasa.gov/mission\\_pages/oco2/](https://www.nasa.gov/mission_pages/oco2/), last access: 18 March 2023; OCO-3, <https://www.jpl.nasa.gov/missions/orbiting-carbon-observatory-3-oco-3>, last access: 18 March 2023) and Greenhouse gases Observing SATellite-2 (GOSAT-2, <https://global.jaxa.jp/projects/sat/gosat2/>, last access: 18 March 2023), as well as the latest reprocessed satellite products from C3S; (ii) improve the underlying anthropogenic emissions and natural fluxes by using the most recent flux data sources, with particular emphasis on the near-real-time extrapolation of the prescribed flux data; (iii) couple the chemical loss rate with the CAMS reanalysis of chemical species (Inness et al., 2019); and (iv) use the IFS inversion capability (McNorton et al., 2022) being developed

within the CoCO2 project (<https://coco2-project.eu>, last access: 18 March 2023) for future reanalyses and explore the possibility of applying a correction to the fluxes in order to match the observed global growth rate.

## Appendix A

**Table A1.** List of stations with in situ continuous observations of CO<sub>2</sub> and CH<sub>4</sub> from GLOBALVIEWplus CO<sub>2</sub> ObsPack v6.0 and CH<sub>4</sub> ObsPack v1.0, respectively, used for the evaluation in Sect. 3.1.

Station, country (site name)	Latitude and longitude	Elevation (m a.s.l.)	Data reference
Alert, Canada (ALT)	82.45° N, 62.51° W	185	Worthy et al. (2003)
Utqiāġvik, AK, USA (BRW)	71.32° N, 156.61° W	11	Peterson et al. (1986)
Candle Lake, Canada (CDL)	53.99° N, 105.12° W	600	Worthy et al. (2003)
Mace Head, Ireland (MHD)	53.33° N, 9.90° W	5	Ramonet et al. (2010)
Fraserdale, Canada (FSD)	49.88° N, 81.57° W	210	Worthy et al. (2003)
Kasprowy Wierch, Poland (KAS)	49.23° N, 19.98° E	1989	Necki et al. (2003)
Schauinsland, Germany (SSL)	47.92° N, 7.92° E	1205	Schmidt et al. (2003)
Hegyhátsál, Hungary (HUN)	46.95° N, 16.65° E	248	Haszpra et al. (2001)
Park Falls, WI, USA (LEF)	45.95° N, 90.27° W	472	Andrews et al. (2014)
Puy de Dôme, France (PUY)	45.77° N, 2.97° E	1465	Lopez et al. (2015), Colomb et al. (2020)
Argyle, ME, USA (AMT)	45.03° N, 68.68° W	53	Andrews et al. (2014)
Sable Island, Canada (WSA)	43.93° N, 60.00° W	5	Worthy et al. (2003)
Ryori, Japan (RYO)	39.03° N, 141.82° E	260	Tsutsumi et al. (2005)
Moody, TX, USA (WKT)	31.31° N, 97.33° W	251	Andrews et al. (2014)
Minamitorishima, Japan (MNM)	24.28° N, 153.98° E	8	Tsutsumi et al. (2005)
Yonagunijima, Japan (YON)	24.47° N, 123.02° E	30	Tsutsumi et al. (2005)
Tutuila, American Samoa, USA (SMO)	14.25° S, 170.56° W	42	Waterman et al. (1989)
Cape Point, South Africa (CPT)	34.35° S, 18.49° E	230	Brunke et al. (2004)
Amsterdam Island, France (AMS)	37.80° S, 77.54° E	55	Ramonet and Monfray (1996)
Baring Head Station, New Zealand (BHD)	41.41° S, 174.87° E	85	Stephens et al. (2013)
Syowa Station, Antarctica (operated by Japan) (SYO)	69.01° S, 39.59° E	14	Schuldt et al. (2020)
South Pole, Antarctica (operated by the USA) (SPO)	89.98° S, 24.8° W	2810	Gillette et al. (1987)

**Table A2.** List of total column stations used for the evaluation in Sect. 3.1.

Station, country	Latitude and longitude	Network	Data references
Eureka, Canada	80.05° N, 86.42° W	TCCON+NDACC	Strong et al. (2019), Batchelor et al. (2009)
Ny Ålesund, Norway	78.9° N, 11.9° E	TCCON+NDACC	Notholt et al. (2019)
Thule, Greenland	76.53° N, 68.74° W	NDACC	Hannigan et al. (2009)
Kiruna, Sweden	67.84° N, 20.41° E	NDACC	Bader et al. (2017)
Sodankylä, Finland	67.37° N, 26.63° E	TCCON+NDACC	Kivi et al. (2014), Sha et al. (2021)
Harestua, Norway	60.2° N, 10.8° E	NDACC	De Mazière et al. (2018)
St Petersburg, Russia	59.90° N 29.80° E	NDACC	Makarova et al. (2015)
East Trout Lake, Canada	54.35° N, 104.99° W	TCCON	Wunch et al. (2018)
Białystok, Poland	53.23° N, 23.02° E	TCCON	Deutscher et al. (2015)
Bremen, Germany	53.1° N, 8.85° E	TCCON	Notholt et al. (2014)
Karlsruhe, Germany	49.1° N, 8.44° E	TCCON	Hase et al. (2015)
Paris, France	48.85° N, 2.36° E	TCCON	Te et al. (2014)
Orléans, France	47.97° N, 2.11° E	TCCON	Warneke et al. (2014)
Garmisch, Germany	47.48° N, 11.06° E	TCCON+NDACC	Sussmann and Rettinger (2018a), Sussmann et al. (2012), Hausmann al. (2016)
Zugspitze, Germany	47.42° N, 10.98° E	TCCON+NDACC	Sussmann and Rettinger (2018b)
Jungfraujoch, Switzerland	46.55° N, 7.98° E	NDACC	Zander et al. (2008)
Park Falls, WI, USA	45.94° N, 90.27° W	TCCON	Wennberg et al. (2017)
Rikubetsu, Japan	43.46° N, 143.77° E	TCCON+NDACC	Morino et al. (2016a), De Mazière et al. (2018)
Boulder, CO, USA	39.99° N, 105.26° W	NDACC	Ortega et al. (2021)
Indianapolis, IN, USA	39.86° N, 86° W	TCCON	Iraci et al. (2016a)
Four Corners, USA	36.8° N, 108.48° W	TCCON	Dubey et al. (2014b)
Lamont, OK, USA	36.5° N, 97.49° W	TCCON	Wennberg et al. (2016a)
Anmyeondo, South Korea	36.54° N, 126.33° E	TCCON	Goo et al. (2014)
Tsukuba, Japan	36.05° N, 140.12° E	TCCON	Morino et al. (2016b)
Nicosia, Cyprus	35.14° N, 33.38° E	TCCON	Petri et al. (2020)
Edwards, CA, USA	34.96° N, 117.88° W	TCCON	Iraci et al. (2016b)
JPL, CA, USA	34.2° N, 118.18° W	TCCON	Wennberg et al. (2016b)
Pasadena Caltech, CA, USA	34.14° N, 118.13° W	TCCON	Wennberg et al. (2015)
Saga, Japan	33.24° N, 130.29° E	TCCON	Kawakami et al. (2014)
Hefei, China	31.9 ° N, 117.17° E	TCCON	Liu et al. (2018)
Izaña, Spain	28.3° N, 16.48° W	TCCON+NDACC	Blumenstock et al. (2014), García et al. (2021)
Mauna Loa, HI, USA	19.54° N, 155.58° W	NDACC	Hannigan et al. (2009)
Altzomoni, Mexico	19.12° N, 98.66° W	NDACC	De Mazière et al. (2018)
Burgos, Philippines	18.53° N, 120.65° E	TCCON	Morino et al. (2018)
Manaus, Brazil	3.21° S, 60.6° W	TCCON	Dubey et al. (2014a)
Ascension Island, UK	7.92° S, 14.33° W	TCCON	Feist et al. (2014)
Darwin, Australia	12.43° S, 130.89° E	TCCON	Griffith et al. (2014a)
Saint-Denis, Réunion, France	20.9° S, 55.49° E	TCCON+NDACC	De Mazière et al. (2014)
Maïdo, Réunion, France	21.1° S, 55.4° E	NDACC	Zhou et al. (2018)
Wollongong, Australia	34.41° S, 150.88° E	TCCON+NDACC	Griffith et al. (2014b), De Mazière et al. (2018)
Lauder, New Zealand	45.05° S, 168.68° E	TCCON+NDACC	Sherlock et al. (2014a, b), Pollard et al. (2019, 2017), Bader et al. (2017)
Arrival Heights, Antarctica	77.83° S, 166.67° E	NDACC	Bader et al. (2017)

**Table A3.** List of AirCore sites (from NOAA\_AirCore\_data\_v20210813; Baier et al., 2021) used for the evaluation in Sect. 3.2.

Site, country	Latitude and longitude
Boulder, CO, USA	40.03° N, 103.74° W
Lamont, OK, USA	36.85° N, 98.21° W
Lauder, New Zealand	45.50° S, 169.47° E
Sodankylä, Finland	67.41° N, 26.31° E
Park Falls, WI, USA	45.97° N, 90.32° W
Edwards, CA, USA	34.65° N, 117.29° W
Traînou, France	48.48° N, 1.16° E

**Code and data availability.** The IFS forecasting and reanalysis system is not for public use as the ECMWF Member States are the proprietary owners. The resulting dataset is however freely available on the Copernicus Atmosphere Data Store. The CAMS GHG reanalysis can be accessed through the CAMS Atmosphere Data Store (ADS) at <https://doi.org/10.24380/8fck-9w87> (Copernicus Atmosphere Monitoring Service, 2021). The format is available in both GRIB and NetCDF. The data record starts on 1 January 2003 at 00:00 UTC and currently stops on 31 December 2020. Recent months will be added over time as soon as the reanalysis procedure and its validation are completed. The original data were available either as spectral coefficients with a triangular truncation of T255 or on a reduced Gaussian grid with a resolution of N128. For the ease of the user, fields were interpolated from their native representation to a regular  $0.75^\circ \times 0.75^\circ$  latitude–longitude grid. For sub-daily data the CAMS reanalysis is archived with a 3-hourly time step (00:00, 03:00, 06:00, 09:00, 12:00, 15:00, 18:00, 21:00 UTC). Precomputed monthly averages are also directly available for all fields. The 3D fields are available on two different vertical resolutions, 25 pressure levels (1000, 950, 925, 900, 850, 800, 700, 600, 500, 400, 300, 250, 200, 150, 100, 70, 50, 30, 20, 10, 7, 5, 3, 2, 1 hPa), and 60 hybrid  $\sigma$ –pressure vertical model levels, which are described at <https://confluence.ecmwf.int/display/UDOC/L60+model+level+definitions> (last access: 18 March 2023). The data records have 18 total 2D radiation fields, two vertically integrated atmospheric datasets of CO<sub>2</sub> and CH<sub>4</sub> (column-mean mole fractions, 14 2D surface flux variables, 32 total 2D meteorological fields, and 16 total 3D fields including meteorological and greenhouse gas fields). A complete listing of the variables included in the CAMS GHG reanalysis is provided in the ADS (<https://ads.atmosphere.copernicus.eu/cdsapp#!/home>, last access: 18 March 2023).

**Supplement.** The supplement related to this article is available online at: <https://doi.org/10.5194/acp-23-3829-2023-supplement>.

**Author contributions.** AAP, JB and SM prepared the manuscript with the rest of the co-authors, monitored the simulation, tested the impact of the surface fluxes, assimilated observations and fixed bugs. AAP was responsible for the forecasting model implementation and performed the evaluation of the vertical profiles and trends. AI led the CAMS reanalysis work and was responsible for

running and monitoring the reanalysis simulations. SM developed the data assimilation of satellite products. MP provided support on the biomass burning emissions and post-processed the fire emission data in Fig. 3. MA worked on documenting the data assimilation aspects of the GHG reanalysis. JF, ZK and LC provided technical support for the diagnostics, implemented bug fixes during the testing stage and tested the CAMS NRT satellite observations. LJ provided technical support with the mass interpolation scheme and diagnostic tools. MihR was responsible for post-processing the dataset into the Copernicus Atmosphere Data Store. RR and MS performed the satellite data acquisition and pre-processing. RE and VHP coordinated the efforts on the CAMS reanalyses. BL, HE, MicR and JT were responsible for validating the reanalysis dataset with independent observations, including the production of surface and column CO<sub>2</sub> and CH<sub>4</sub> evaluation plots. IA, TB, MB, CC, OH, NM, SN, MaR and LW provided support for the use of the satellite retrieval products. All authors reviewed and edited the manuscript.

**Competing interests.** The contact author has declared that none of the authors has any competing interests.

**Disclaimer.** Publisher's note: Copernicus Publications remains neutral with regard to jurisdictional claims in published maps and institutional affiliations.

**Acknowledgements.** The satellite data assimilated in the CAMS GHG reanalysis were obtained from the ESA GHG-CCI project (<https://climate.esa.int/en/projects/ghgs/Data>, last access: 18 March 2023) and the Copernicus Climate Change Service (C3S) Climate Data Store (<https://cds.climate.copernicus.eu>, last access: 18 March 2023). The data used to evaluate the CAMS GHG reanalysis were obtained from the Total Carbon Column Observing Network (TCCON) Data Archive hosted by CaltechDATA at <https://tccondat.org> (last access: 18 March 2023). CH<sub>4</sub> data were obtained from the Network for the Detection of Atmospheric Composition Change (NDACC, <https://www.ndacc.org>, last access: 18 March 2023; Sussmann et al., 2011, 2013; De Mazière et al., 2018) (see Table A2), the Observation Package (ObsPack) GLOBALVIEW-plus Data Products <https://gml.noaa.gov/ccgg/obspack> (last access: 18 March 2023), the NOAA AirCore dataset <https://gml.noaa.gov/ccgg/arc/?id=144> (last access: 18 March 2023), and the NOAA Greenhouse Gas Marine Boundary Layer Reference <https://gml.noaa.gov/ccgg/mbl/mbl.html> (last access: 18 March 2023).

For the NDACC data, the National Center for Atmospheric Research is sponsored by the National Science Foundation. The NCAR FTS observation programmes at Thule, Greenland; Boulder, CO, USA; and Mauna Loa, HI, USA, are supported under contract by the National Aeronautics and Space Administration (NASA). The Thule work is also supported by the NSF Office of Polar Programs (OPP). We wish to thank the Danish Meteorological Institute for their support at the Thule site and NOAA for their support of the Mauna Loa site. The multi-decadal monitoring programme of the University of Liège at the Jungfraujoch station has been primarily supported by the F.R.S.-FNRS and BELSPO (both in Brussels, Belgium) and by the GAW-CH programme of MeteoSwiss. The International Foundation High Altitude Research Stations Jungfrau-

joch and Gornergrat (HFSJG, Bern) supported the facilities needed to perform the FTIR observations at Jungfraujoch.

The authors are also grateful to László Haszpra for his comments on the Hegyhátsál tall-tower station, Xin Lan and Ed Dlugokencky for the feedback on the use of NOAA/GML MBL data, and Debra Wunch for providing insight into the potential impact of polar vortex on the XCH<sub>4</sub> data at the East Trout Lake TCCON site.

**Financial support.** The CAMS GHG reanalysis has been funded by the Copernicus Atmosphere Monitoring Service, which is operated by the European Centre for Medium-Range Weather Forecasts on behalf of the European Commission as part of the Copernicus Programme (<http://copernicus.eu>, last access: 18 March 2023).

**Review statement.** This paper was edited by Aurélien Podglajen and reviewed by Saroja Polavarapu and two anonymous referees.

## References

- Agustí-Panareda, A., Massart, S., Chevallier, F., Balsamo, G., Boussetta, S., Dutra, E., and Beljaars, A.: A biogenic CO<sub>2</sub> flux adjustment scheme for the mitigation of large-scale biases in global atmospheric CO<sub>2</sub> analyses and forecasts, *Atmos. Chem. Phys.*, 16, 10399–10418, <https://doi.org/10.5194/acp-16-10399-2016>, 2016.
- Agustí-Panareda, A., Diamantakis, M., Bayona, V., Klappenbach, F., and Butz, A.: Improving the inter-hemispheric gradient of total column atmospheric CO<sub>2</sub> and CH<sub>4</sub> in simulations with the ECMWF semi-Lagrangian atmospheric global model, *Geosci. Model Dev.*, 10, 1–18, <https://doi.org/10.5194/gmd-10-1-2017>, 2017.
- Agustí-Panareda, A., Diamantakis, M., Massart, S., Chevallier, F., Muñoz-Sabater, J., Barré, J., Curcoll, R., Engelen, R., Langrock, B., Law, R. M., Loh, Z., Morguí, J. A., Parrington, M., Peuch, V.-H., Ramonet, M., Roehl, C., Vermeulen, A. T., Warneke, T., and Wunch, D.: Modelling CO<sub>2</sub> weather – why horizontal resolution matters, *Atmos. Chem. Phys.*, 19, 7347–7376, <https://doi.org/10.5194/acp-19-7347-2019>, 2019.
- Agustí-Panareda, A., McNorton, J., Balsamo, G., Baier, B. C., Bouscerez, N., Boussetta, S., Brunner, D., Chevallier, F., Choulga, M., Diamantakis, M., Engelen, R., Flemming, J., Granier, C., Guevara, M., Denier van der Gon, H., Elguindi, N., Haussaire, J.-M., Jung, M., Janssens-Maenhout, G., Kivi, R., Massart, S., Papale, D., Parrington, M., Razinger, M., Sweeney, C., Vermeulen, A., and Walther, S.: Global nature run data with realistic high-resolution carbon weather for the year of the Paris Agreement, *Sci. Data*, 9, 160, <https://doi.org/10.1038/s41597-022-01228-2>, 2022.
- Alos, A. L., Bergeron, C., Buontempo, C., Thepaut, J. N., Raoult, B., and Biavati, G.: The Copernicus Climate Data Store: ECMWF's approach to providing online access to climate data and tools, AGU Fall Meeting 2019, 9–13 December 2019, San Francisco, CA, USA, AGU Fall Meeting Abstracts, vol. 2019, PA31A-05, 2019.
- Andrews, A. E., Kofler, J. D., Trudeau, M. E., Williams, J. C., Neff, D. H., Masarie, K. A., Chao, D. Y., Kitzis, D. R., Novelli, P. C., Zhao, C. L., Dlugokencky, E. J., Lang, P. M., Crotwell, M. J., Fischer, M. L., Parker, M. J., Lee, J. T., Baumann, D. D., Desai, A. R., Stanier, C. O., De Wekker, S. F. J., Wolfe, D. E., Munger, J. W., and Tans, P. P.: CO<sub>2</sub>, CO, and CH<sub>4</sub> measurements from tall towers in the NOAA Earth System Research Laboratory's Global Greenhouse Gas Reference Network: instrumentation, uncertainty analysis, and recommendations for future high-accuracy greenhouse gas monitoring efforts, *Atmos. Meas. Tech.*, 7, 647–687, <https://doi.org/10.5194/amt-7-647-2014>, 2014.
- Bader, W., Bovy, B., Conway, S., Strong, K., Smale, D., Turner, A. J., Blumenstock, T., Boone, C., Collaud Coen, M., Coulon, A., Garcia, O., Griffith, D. W. T., Hase, F., Hausmann, P., Jones, N., Krummel, P., Murata, I., Morino, I., Nakajima, H., O'Doherty, S., Paton-Walsh, C., Robinson, J., Sandrin, R., Schneider, M., Servais, C., Sussmann, R., and Mahieu, E.: The recent increase of atmospheric methane from 10 years of ground-based NDACC FTIR observations since 2005, *Atmos. Chem. Phys.*, 17, 2255–2277, <https://doi.org/10.5194/acp-17-2255-2017>, 2017.
- Baier, B., Sweeney, C., Newberger, T., Higgs, J., Wolter, S., and NOAA Global Monitoring Laboratory: NOAA AirCore atmospheric sampling system profiles (Version 20210813), NOAA GML [data set], <https://doi.org/10.15138/6AV0-MY81>, 2021.
- Batchelor, R. L., Strong, K., Lindenmaier, R., Mittermeier, R. L., Fast, H., Drummond, J. R., and Fogal, P. F.: A New Bruker IFS 125HR FTIR Spectrometer for the Polar Environment Atmospheric Research Laboratory at Eureka, Nunavut, Canada: Measurements and Comparison with the Existing Bomem DA8 Spectrometer, *J. Atmos. Ocean. Tech.*, 26, 1328–1340, <https://doi.org/10.1175/2009TECHA1215.1>, 2009.
- Bechtold, P., Semane, N., Lopez, P., Chaboureau, J.-P., Beljaars, A., and Bormann, N.: Representing Equilibrium and Nonequilibrium Convection in Large-Scale Models, *J. Atmos. Sci.*, 71, 734–753, 2014.
- Bergamaschi, P., Krol, M., Dentener, F., Vermeulen, A., Meinhardt, F., Graul, R., Ramonet, M., Peters, W., and Dlugokencky, E. J.: Inverse modelling of national and European CH<sub>4</sub> emissions using the atmospheric zoom model TM5, *Atmos. Chem. Phys.*, 5, 2431–2460, <https://doi.org/10.5194/acp-5-2431-2005>, 2005.
- Bergamaschi, P., Frankenberg, C., Meirink, J. F., Krol, M., Villani, G., Houweling, S., Dentener, F., Dlugokencky, E. J., Miller, J. B., Gatti, L. V., Engel, A., and Levin, I.: Inverse modeling of global and regional CH<sub>4</sub> emissions using SCIAMACHY satellite retrievals, *J. Geophys. Res.-Atmos.*, 114, D22301, <https://doi.org/10.1029/2009JD012287>, 2009.
- Blumenstock, T., Hase, F., Schneider, M., Garcia, O., and Sepulveda, E.: TCCON data from Izana (ES), Release GGG2014.R0 (Version GGG2014.R0), CaltechDATA [data set], <https://doi.org/10.14291/TCCON.GGG2014.IZANA01.R0/1149295>, 2014.
- Boussetta, S., Balsamo, G., Beljaars, A., Agustí-Panareda, A., Calvet, J. C., Jacobs, C., van den Hurk, B., Viterbo, P., Lafont, S., and Dutra, E.: Natural land carbon dioxide exchanges in the ECMWF integrated forecasting system: Implementation and offline validation, *J. Geophys. Res.-Atmos.*, 118, 5923–5946, 2013.
- Brühl, C. and Crutzen, P. J.: The MPIC 2D model, *NASA Ref. Publ.*, 1292, 103–104, 1993.
- Brunke, E.-G., Labuschagne, C., Parker, B., Scheel, H. E., and Whittlestone, S.: Baseline air mass selection at Cape Point, South Africa: Application of <sup>222</sup>Rn and other filter criteria to CO<sub>2</sub>, *Atmos. Environ.*, 38, 5693–5702, 2004.

- Buchwitz, M., Reuter, M., Schneising, O., Boesch, H., Guerlet, S., Dils, B., Aben, I., Armante, R., Bergamaschi, P., Blumenstock, T., Bovensmann, H., Brunner, D., Buchmann, B., Burrows, J., Butz, A., Chédin, A., Chevallier, F., Crevoisier, C., Deutscher, N., Frankenberg, C., Hase, F., Hasekamp, O., Heymann, J., Kaminski, T., Laeng, A., Lichtenberg, G., Demazière, M., Noël, S., Notholt, J., Orphal, J., Popp, C., Parker, R., Scholze, M., Sussmann, R., Stiller, G., Warneke, T., Zehner, C., Bril, A., Crisp, D., Griffith, D., Kuze, A., O'Dell, C., Oshchepkov, S., Sherlock, V., Suto, H., Wennberg, P., Wunch, D., Yokota, T., and Yoshida, Y.: The Greenhouse Gas Climate Change Initiative (GHG-CCI): Comparison and quality assessment of near-surface-sensitive satellite-derived CO<sub>2</sub> and CH<sub>4</sub> global data sets, *Remote Sens. Environ.*, 162, 344–362, 2015.
- Butz, A., Hasekamp, O. P., Frankenberg, C., Vidot, J., and Aben, I.: CH<sub>4</sub> retrievals from space-based solar backscatter measurements: Performance evaluation against simulated aerosol and cirrus loaded scenes, *J. Geophys. Res.*, 115, D24302, <https://doi.org/10.1029/2010JD014514>, 2010.
- Butz, A., Guerlet, S., Hasekamp, O., Schepers, D., Galli, A., Aben, I., Frankenberg, C., Hartmann, J.-M., Tran, H., Kuze, A., Keppel-Aleks, G., Toon, G., Wunch, D., Wennberg, P., Deutscher, N., Griffith, D., Macatangay, R., Messerschmidt, J., Notholt, J., and Warneke, T.: Toward accurate CO<sub>2</sub> and CH<sub>4</sub> observations from GOSAT, *Geophys. Res. Lett.*, 38, L14812, <https://doi.org/10.1029/2011GL047888>, 2011.
- Chevallier, F.: Description of the CO<sub>2</sub> inversion production chain 2020, Copernicus Atmosphere Monitoring Service, [https://atmosphere.copernicus.eu/sites/default/files/2020-06/CAMS73\\_2018SC2\\_%20D5.2.1-2020\\_202004\\_%20CO2%20inversion%20production%20chain\\_v1.pdf](https://atmosphere.copernicus.eu/sites/default/files/2020-06/CAMS73_2018SC2_%20D5.2.1-2020_202004_%20CO2%20inversion%20production%20chain_v1.pdf) (last access: 18 March 2023), 2020.
- Chevallier, F., Ciais, P., Conway, T. J., Aalto, T., Anderson, B. E., Bousquet, P., Brunke, E. G., Ciattaglia, L., Esaki, Y., Fröhlich, M., Gomez, A., Gomez-Pelaez, A. J., Haszpra, L., Krummel, P. B., Langenfelds, R. L., Leuenberger, M., Machida, T., Maignan, F., Matsueda, H., Morguí, J. A., Mukai, H., Nakazawa, T., Peylin, P., Ramonet, M., Rivier, L., Sawa, Y., Schmidt, M., Steele, L. P., Vay, S. A., Vermeulen, A. T., Wofsy, S., and Worthy, D.: CO<sub>2</sub> surface fluxes at grid point scale estimated from a global 21-year reanalysis of atmospheric measurements, *J. Geophys. Res.*, 115, D21307, <https://doi.org/10.1029/2010JD013887>, 2010.
- Chevallier, F., Remaud, M., O'Dell, C. W., Baker, D., Peylin, P., and Cozic, A.: Objective evaluation of surface- and satellite-driven carbon dioxide atmospheric inversions, *Atmos. Chem. Phys.*, 19, 14233–14251, <https://doi.org/10.5194/acp-19-14233-2019>, 2019.
- Colomb, A., Delmotte, M., Pichon, J., Ramonet, M., and Yver-Kwok, C.: ICOS RI, 2020, ICOS ATC CO<sub>2</sub> Release, Puy de Dôme (10.0 m), 2016-08-25–2020-05-31, ICOS Carbon Portal, <https://hdl.handle.net/11676/xMV5-Hxu7bA9q872kedNJIaf> (last access: 18 March 2023), 2020.
- Conway, T. J., Tans, P. P., Waterman, L. S., Thoning, K. W., Kitzis, D. R., Masarie, K. A., and Zhang, N.: Evidence for interannual variability of the carbon cycle from the NOAA/CMDL global air sampling network, *J. Geophys. Res.*, 99, 22831–22855, 1994.
- Cooperative Global Atmospheric Data Integration Project: Multi-laboratory compilation of atmospheric methane data for the period 1957–2017; ob-
- spack\_ch4\_1\_GLOBALVIEWplus\_v1.0\_2019\_01\_08, NOAA Earth System Research Laboratory, Global Monitoring Division, <https://doi.org/10.25925/20190108>, 2019.
- Copernicus Atmosphere Monitoring Service: CAMS global greenhouse gas reanalysis (EGG4), CAMS Atmosphere Data Store (ADS) [data set], <https://doi.org/10.24380/8fck-9w87>, 2021.
- Crevoisier, C., Chédin, A., Matsueda, H., Machida, T., Armante, R., and Scott, N. A.: First year of upper tropospheric integrated content of CO<sub>2</sub> from IASI hyperspectral infrared observations, *Atmos. Chem. Phys.*, 9, 4797–4810, <https://doi.org/10.5194/acp-9-4797-2009>, 2009a.
- Crevoisier, C., Nobileau, D., Fiore, A. M., Armante, R., Chédin, A., and Scott, N. A.: Tropospheric methane in the tropics – first year from IASI hyperspectral infrared observations, *Atmos. Chem. Phys.*, 9, 6337–6350, <https://doi.org/10.5194/acp-9-6337-2009>, 2009b.
- Crevoisier, C., Clerbaux, C., Guidard, V., Phulpin, T., Armante, R., Barret, B., Camy-Peyret, C., Chaboureau, J.-P., Coheur, P.-F., Crépeau, L., Dufour, G., Labonne, L., Lavanant, L., Hadji-Lazaro, J., Herbin, H., Jacquinet-Husson, N., Payan, S., Péquignot, E., Pierangelo, C., Sellitto, P., and Stubenrauch, C.: Towards IASI-New Generation (IASI-NG): impact of improved spectral resolution and radiometric noise on the retrieval of thermodynamic, chemistry and climate variables, *Atmos. Meas. Tech.*, 7, 4367–4385, <https://doi.org/10.5194/amt-7-4367-2014>, 2014.
- Crisp, D., Meijer, Y., Munro, R., Bowman, K., Chatterjee, A., Baker, D., Chevallier, F., Nassar, R., Palmer, P. I., Agustí-Panareda, A., Al-Saadi, J., Ariel, Y., Basu, S., Bergamaschi, P., Boesch, H., Bousquet, P., Bovensmann, H., Breton, F. M., Brunner, D., Buchwitz, M., Buisson, F., Burrows, J. P., Butz, A., Ciais, P., Clerbaux, C., Counet, P., Crevoisier, C., Crowell, S., DeCola, P. L., Deniel, C., Dowell, M., Eckman, R., Edwards, D., Ehret, G., Eldering, A., Engelen, R., Fisher, B., Germain, S., Hakkarainen, J., Hilsenrath, E., Holmlund, K., Houweling, S., Hu, H., Jacob, D., Janssens-Maenhout, G., Jones, D., Jouget, D., Kataoka, F., Kiel, M., Kulawik, S. S., Kuze, A., Lachance, R. L., Lang, R., Landgraf, L., Liu, J., Liu, Y., Maksyutov, S., Matsunaga, T., McKeever, J., Moore, B., Nakajima, M., Natraj, V., Nelson, R. R., Niwa, Y., Oda, T., O'Dell, C. W., Ott, L., Patra, P., Pawson, S., Payne, V., Pinty, B., Polavarapu, S. M., Retscher, C., Rosenberg, R., Schuh, A., Schwandner, F. M., Shiomi, K., Su, W., Tamminen, J., Taylor, T. E., Veefkind, P., Veihelmann, B., Wofsy, S., Worden, J., Wunch, D., Yang, D., Zhang, P., and Zehner, C.: A constellation architecture for monitoring carbon dioxide and methane from space, CEOS Atmospheric Composition Virtual Constellation Greenhouse Gas Team Rep., 173 pp., [http://ceos.org/document\\_management/Virtual\\_Constellations/ACC/Documents/CEOS\\_AC-VC\\_GHG\\_White\\_Paper\\_Version\\_1\\_20181009.pdf](http://ceos.org/document_management/Virtual_Constellations/ACC/Documents/CEOS_AC-VC_GHG_White_Paper_Version_1_20181009.pdf) (last access: 18 March 2023), 2018.
- De Mazière, M., Sha, M. K., Desmet, F., Hermans, C., Scolas, F., Kumps, N., Metzger, J.-M., Duflat, V., and Cammas, J.-P.: TCCON data from Réunion Island (RE), Release GGG2014.R0 (Version GGG2014.R0), CaltechDATA [data set], <https://doi.org/10.14291/tcon.ggg2014.reunion01.R0/1149288>, 2014.
- De Mazière, M., Thompson, A. M., Kurylo, M. J., Wild, J. D., Bernhard, G., Blumenstock, T., Braathen, G. O., Hannigan, J. W., Lambert, J.-C., Leblanc, T., McGee, T. J., Nedoluha, G., Petropavlovskikh, I., Seckmeyer, G., Simon, P. C., Stein-

- brecht, W., and Strahan, S. E.: The Network for the Detection of Atmospheric Composition Change (NDACC): history, status and perspectives, *Atmos. Chem. Phys.*, 18, 4935–4964, <https://doi.org/10.5194/acp-18-4935-2018>, 2018.
- Deutscher, N. M., Notholt, J., Messerschmidt, J., Weinzierl, C., Warneke, T., Petri, C., and Grupe, P.: TCCON data from Bialystok (PL), Release GGG2014.R1 (Version GGG2014.R1), CaltechDATA [data set], <https://doi.org/10.14291/TCCON.GGG2014.BIALYSTOK1.R1/1183984>, 2015.
- Diamantakis, M. and Agustí-Panareda, A.: A positive definite tracer mass fixer for high resolution weather and atmospheric composition forecasts, ECMWF Technical Memoranda, 819, <https://www.ecmwf.int/en/elibrary/80422-positive-definite-tracer-mass-fixer-high-resolution-weather-and-atmospheric> (last access: 18 March 2023), 2017.
- Diamantakis, M. and Magnusson, L.: Sensitivity of the ECMWF Model to Semi-Lagrangian Departure Point Iterations, *Mon. Weather Rev.*, 144, 3233–3250, 2016.
- Doumbia, T., Granier, C., Elguindi, N., Bouarar, I., Darras, S., Brasseur, G., Gaubert, B., Liu, Y., Shi, X., Stavrakou, T., Tilmes, S., Lacey, F., Deroubaix, A., and Wang, T.: Changes in global air pollutant emissions during the COVID-19 pandemic: a dataset for atmospheric modeling, *Earth Syst. Sci. Data*, 13, 4191–4206, <https://doi.org/10.5194/essd-13-4191-2021>, 2021.
- Slagter, E. J., Steele, L. P., Lang, P. M., and Masarie, K. A.: The growth rate and distribution of atmospheric methane, *J. Geophys. Res.*, 99, 17021–17043, 1994.
- Slagter, E. J., Mund, J. W., Crotwell, A. M., Crotwell, M. J., and Thoning, K. W.: Atmospheric Carbon Dioxide Dry Air Mole Fractions from the NOAA GML Carbon Cycle Cooperative Global Air Sampling Network, 1968–2020, Version: 2021-07-30, NOAA Global Monitoring Laboratory Data Repository, <https://doi.org/10.15138/wkgj-f215>, 2021.
- Dubey, M. K., Henderson, B. G., Green, D., Butterfield, Z. T., Keppel-Aleks, G., Allen, N. T., Blavier, J.-F., Roehl, C. M., Wunch, D., and Lindenmaier, R.: TCCON data from Manaus (BR), Release GGG2014.R0 (Version GGG2014.R0), CaltechDATA [data set], <https://doi.org/10.14291/tcon.ggg2014.manaus01.R0/1149274>, 2014a.
- Dubey, M. K., Lindenmaier, R., Henderson, B. G., Green, D., Allen, N. T., Roehl, C. M., Blavier, J.-F., Butterfield, Z. T., Love, S., Hamelmann, J. D., and Wunch, D.: TCCON data from Four Corners, NM, USA, Release GGG2014R0, TCCON data archive, hosted by CaltechDATA, California Institute of Technology, Pasadena, CA, USA [data set], <https://doi.org/10.14291/tcon.ggg2014.fourcorners01.R0/1149272>, 2014b.
- Feist, D. G., Arnold, S. G., John, N., and Geibel, M. C.: TCCON data from Ascension Island (SH), Release GGG2014.R0 (Version GGG2014.R0), CaltechDATA [data set], <https://doi.org/10.14291/TCCON.GGG2014.ASCENSION01.R0/1149285>, 2014.
- Fisher, M.: Generalized frames on the sphere with application to background error covariance modelling, Seminar on recent developments in numerical methods for atmospheric and ocean modelling, 6–10 September 2004, Shinfield Park, Reading, UK, Proceedings, ECMWF, Reading, UK, 87–101, <https://www.ecmwf.int/en/elibrary/74484-generalized-frames-sphere-application-background-error-covariance-modelling> (last access: 18 March 2023), 2004.
- Fisher, M.: Wavelet Jb – A new way to model the statistics of background errors, ECMWF Newsletter, 106, 23–28, ECMWF, Reading, UK, <https://doi.org/10.21957/ef5601ak43>, 2006.
- Flemming, J., Huijnen, V., Arteta, J., Bechtold, P., Beljaars, A., Blechschmidt, A.-M., Diamantakis, M., Engelen, R. J., Gaudel, A., Inness, A., Jones, L., Josse, B., Katragkou, E., Marecal, V., Peuch, V.-H., Richter, A., Schultz, M. G., Stein, O., and Tsikkerdekkis, A.: Tropospheric chemistry in the Integrated Forecasting System of ECMWF, *Geosci. Model Dev.*, 8, 975–1003, <https://doi.org/10.5194/gmd-8-975-2015>, 2015.
- Frankenberg, C., Aben, I., Bergamaschi, P., Dlugokencky, E. J., van Hees, R., Houweling, S., van der Meer, P., Snel, R., and Tol, P.: Global column-averaged methane mixing ratios from 2003 to 2009 as derived from SCIAMACHY: trends and variability, *J. Geophys. Res.-Atmos.*, 116, D04302, <https://doi.org/10.1029/2010JD014849>, 2011.
- Friedlingstein, P., Jones, M. W., O'Sullivan, M., Andrew, R. M., Bakker, D. C. E., Hauck, J., Le Quéré, C., Peters, G. P., Peters, W., Pongratz, J., Sitch, S., Canadell, J. G., Ciais, P., Jackson, R. B., Alin, S. R., Anthoni, P., Bates, N. R., Becker, M., Bellouin, N., Bopp, L., Chau, T. T. T., Chevallier, F., Chini, L. P., Cronin, M., Currie, K. I., Decharme, B., Djeutchouang, L. M., Dou, X., Evans, W., Feely, R. A., Feng, L., Gasser, T., Gilfillan, D., Gkrizalis, T., Grassi, G., Gregor, L., Gruber, N., Gürses, Ö., Harris, I., Houghton, R. A., Hurtt, G. C., Iida, Y., Ilyina, T., Luijkx, I. T., Jain, A., Jones, S. D., Kato, E., Kennedy, D., Klein Goldewijk, K., Knauer, J., Korsbakken, J. I., Kötzinger, A., Landschützer, P., Lauvset, S. K., Lefèvre, N., Lienert, S., Liu, J., Marland, G., McGuire, P. C., Melton, J. R., Munro, D. R., Nabel, J. E. M. S., Nakao, S.-I., Niwa, Y., Ono, T., Pierrot, D., Poulter, B., Rehder, G., Resplandy, L., Robertson, E., Rödenbeck, C., Rosan, T. M., Schwinger, J., Schwingshackl, C., Séférian, R., Sutton, A. J., Sweeney, C., Tanhua, T., Tans, P. P., Tian, H., Tilbrook, B., Tubiello, F., van der Werf, G. R., Vuichard, N., Wada, C., Wanninkhof, R., Watson, A. J., Willis, D., Wiltshire, A. J., Yuan, W., Yue, C., Yue, X., Zaehle, S., and Zeng, J.: Global Carbon Budget 2021, *Earth Syst. Sci. Data*, 14, 1917–2005, <https://doi.org/10.5194/essd-14-1917-2022>, 2022.
- García, O. E., Schneider, M., Sepúlveda, E., Hase, F., Blumenstock, T., Cuevas, E., Ramos, R., Gross, J., Barthlott, S., Röhling, A. N., Sanromá, E., González, Y., Gómez-Peláez, Á. J., Navarro-Comas, M., Puentedura, O., Yela, M., Redondas, A., Carreño, V., León-Luis, S. F., Reyes, E., García, R. D., Rivas, P. P., Romero-Campos, P. M., Torres, C., Prats, N., Hernández, M., and López, C.: Twenty years of ground-based NDACC FTIR spectrometry at Izaña Observatory – overview and long-term comparison to other techniques, *Atmos. Chem. Phys.*, 21, 15519–15554, <https://doi.org/10.5194/acp-21-15519-2021>, 2021.
- Gillette, D. A., Komhyr, W. D., Waterman, L. S., Steele, L. P., and Gammon, R. H.: The NOAA/GMCC continuous CO<sub>2</sub> record at the South Pole, 1975–1982, *J. Geophys. Res.*, 92, 4231–4240, <https://doi.org/10.1029/JD092iD04p04231>, 1987.
- Goo, T.-Y., Oh, Y.-S., and Velazco, V. A.: TCCON data from Anmeyondo (KR), Release GGG2014.R0 (Version GGG2014.R0), CaltechDATA [data set], <https://doi.org/10.14291/TCCON.GGG2014.ANMEYONDO01.R0/1149284>, 2014.
- Griffith, D. W. T., Deutscher, N. M., Velazco, V. A., Wennberg, P. O., Yavin, Y., Keppel-Aleks, G., Washenfelder, R. A., Toon, G. C., Blavier, J.-F., Paton-Walsh, C., Jones, N. B., Ket-

- tlewell, G. C., Connor, B. J., Macatangay, R. C., Roehl, C., Ryczek, M., Glowacki, J., Culgan, T., and Bryant, G. W.: TCCON data from Darwin (AU), Release GGG2014.R0 (Version GGG2014.R0), CaltechDATA [data set], <https://doi.org/10.14291/TCCON.GGG2014.DARWIN01.R0/1149290>, 2014a.
- Griffith, D. W. T., Velazco, V. A., Deutscher, N. M., Paton-Walsh, C., Jones, N. B., Wilson, S. R., Macatangay, R. C., Kettlewell, G. C., Buschholz, R. R., and Rigganbach, M. O.: TCCON data from Wollongong (AU), Release GGG2014.R0 (Version GGG2014.R0), CaltechDATA [data set], <https://doi.org/10.14291/tcccon.ggg2014.wollongong01.R0/1149291>, 2014b.
- Guerlet, S., Butz, A., Schepers, D., Basu, S., Hasekamp, O. P., Kuze, A., Yokota, T., Blavier, J.-F., Deutscher, N. M., Griffith, D. W., Hase, F., Kyro, E., Morino, I., Sherlock, V., Sussmann, R., Galli, A., and Aben, I.: Impact of aerosol and thin cirrus on retrieving and validating XCO<sub>2</sub> from GOSAT shortwave infrared measurements, *J. Geophys. Res.-Atmos.*, 118, 4887–4905, <https://doi.org/10.1002/jgrd.50332>, 2013.
- Hannigan, J. W., Coffey, M. T., and Goldman, A.: Semiautonomous FTS Observation System for Remote Sensing of Stratospheric and Tropospheric Gases, *J. Atmos. Ocean. Tech.*, 26, 1814–1828, <https://doi.org/10.1175/2009JTECHA1230.1>, 2009.
- Hase, F., Blumenstock, T., Dohe, S., Gros, J., and Kiel, M.: TCCON data from Karlsruhe (DE), Release GGG2014.R1 (Version GGG2014.R1), CaltechDATA [data set], <https://doi.org/10.14291/TCCON.GGG2014.KARLSRUHE01.R1/1182416>, 2015.
- Haszpra, L., Barcza, Z., Bakwin, P. S., Berger, B. W., Davis, K. J., and Weidinger, T.: Measuring system for the long-term monitoring of biosphere/atmosphere exchange of carbon dioxide, *J. Geophys. Res.*, 106D, 3057–3070, 2001.
- Hausmann, P., Sussmann, R., and Smale, D.: Contribution of oil and natural gas production to renewed increase in atmospheric methane (2007–2014): top-down estimate from ethane and methane column observations, *Atmos. Chem. Phys.*, 16, 3227–3244, <https://doi.org/10.5194/acp-16-3227-2016>, 2016.
- Hersbach, H., Bell, B., Berrisford, P., Hirahara, S., Horányi, A., Muñoz-Sabater, J., Nicolas, J., Peubey, C., Radu, R., Schepers, D., Simmons, A., Soci, C., Abdalla, S., Abellán, X., Balsamo, G., Bechtold, P., Biavati, G., Bidlot, J., Bonavita, M., De Chiara, G., Dahlgren, P., Dee, D., Diamantakis, M., Dragani, R., Flemming, J., Forbes, R., Fuentes, M., Geer, A., Haimberger, L., Healy, S., Hogan, R. J., Hölm, E., Janisková, M., Keeley, S., Laloyaux, P., Lopez, P., Lupu, C., Radnoti, G., de Rosnay, P., Rozum, I., Vamborg, F., Villaume, S., and Thépaut, J. N.: The ERA5 global reanalysis, *Q. J. Roy. Meteor. Soc.*, 146, 1999–2049, 2020.
- Heymann, J., Reuter, M., Hilker, M., Buchwitz, M., Schneising, O., Bovensmann, H., Burrows, J. P., Kuze, A., Suto, H., Deutscher, N. M., Dubey, M. K., Griffith, D. W. T., Hase, F., Kawakami, S., Kivi, R., Morino, I., Petri, C., Roehl, C., Schneider, M., Sherlock, V., Sussmann, R., Velazco, V. A., Warneke, T., and Wunch, D.: Consistent satellite XCO<sub>2</sub> retrievals from SCIAMACHY and GOSAT using the BESD algorithm, *Atmos. Meas. Tech.*, 8, 2961–2980, <https://doi.org/10.5194/amt-8-2961-2015>, 2015.
- Houweling, S., Dentener, F., and Lelieveld, J.: The impact of nonmethane hydrocarbon compounds on tropospheric photochemistry, *J. Geophys. Res.*, 103, 10673–10696, <https://doi.org/10.1029/97JD03582>, 1998.
- Houweling, S., Kaminski, T., Dentener, F., Lelieveld, J., and Heimann, M.: Inverse modeling of methane sources and sinks using the adjoint of a global transport model, *J. Geophys. Res.-Atmos.*, 104, 26137–26160, 1999.
- Inness, A., Ades, M., Agustí-Panareda, A., Barré, J., Benedictow, A., Blechschmidt, A.-M., Dominguez, J. J., Engelen, R., Eskes, H., Flemming, J., Huijnen, V., Jones, L., Kipling, Z., Massart, S., Parrington, M., Peuch, V.-H., Razinger, M., Remy, S., Schulz, M., and Suttie, M.: The CAMS reanalysis of atmospheric composition, *Atmos. Chem. Phys.*, 19, 3515–3556, <https://doi.org/10.5194/acp-19-3515-2019>, 2019.
- IPCC: Summary for Policymakers, in: Climate Change 2021: The Physical Science Basis, Contribution of Working Group I to the Sixth Assessment Report of the Intergovernmental Panel on Climate Change, edited by: Masson-Delmotte, V., Zhai, P., Pirani, A., Connors, S. L., Péan, C., Berger, S., Caud, N., Chen, Y., Goldfarb, L., Gomis, M. I., Huang, M., Leitzell, K., Lonnoy, E., Matthews, J. B. R., Maycock, T. K., Waterfield, T., Yelekçi, O., Yu, R., and Zhou, B., Cambridge University Press, in press, 2021.
- Iraci, L., Podolske, J., Hillyard, P., Roehl, C., Wennberg, P. O., Blavier, J.-F., Landeros, J., Allen, N., Wunch, D., Zavaleta, J., Quigley, E., Osterman, G., Barrow, E., and Barney, J.: TCCON data from Indianapolis, Indiana, USA, Release GGG2014R1, TCCON data archive, hosted by CaltechDATA, California Institute of Technology, Pasadena, CA, USA [data set], <https://doi.org/10.14291/tcccon.ggg2014.indianapolis01.R1/1330094>, 2016a.
- Iraci, L. T., Podolske, J. R., Hillyard, P. W., Roehl, C., Wennberg, P. O., Blavier, J.-F., Landeros, J., Allen, N., Wunch, D., Zavaleta, J., Quigley, E., Osterman, G. B., Albertson, R., Dunwoody, K., and Boyden, H.: TCCON data from Edwards (US), Release GGG2014.R1 (Version GGG2014.R1), CaltechDATA [data set], <https://doi.org/10.14291/TCCON.GGG2014.EDWARDS01.R1/1255068>, 2016b.
- Janssens-Maenhout, G., Crippa, M., Guizzardi, D., Muntean, M., and Schaaf, E.: Emissions Database for Global Atmospheric Research, version v4.2 (time-series), European Commission, Joint Research Centre (JRC) [data set], <http://data.europa.eu/89h/jrc-edgar-emissiontimeseriesv42> (last access: 18 March 2023), 2011.
- Janssens-Maenhout, G., Crippa, M., Guizzardi, D., Muntean, M., and Schaaf, E.: JRC-EDGARv431\_AP\_timeseries, European Commission, Joint Research Centre (JRC) [data set], [http://data.europa.eu/89h/jrc-edgar-edgar\\_v431\\_timeseries](http://data.europa.eu/89h/jrc-edgar-edgar_v431_timeseries) (last access: 18 March 2023), 2016.
- Kaiser, J. W., Heil, A., Andreae, M. O., Benedetti, A., Chubarova, N., Jones, L., Morcrette, J.-J., Razinger, M., Schultz, M. G., Suttie, M., and van der Werf, G. R.: Biomass burning emissions estimated with a global fire assimilation system based on observed fire radiative power, *Biogeosciences*, 9, 527–554, <https://doi.org/10.5194/bg-9-527-2012>, 2012.
- Karion, A., Sweeney, C., Tans, P., and Newberger, T.: AirCore: An Innovative Atmospheric Sampling System, *J. Atmos. Ocean. Tech.*, 27, 1839–1843, <https://doi.org/10.1175/2010JTECHA1448.1>, 2010.
- Kawakami, S., Ohyama, H., Arai, K., Okumura, H., Taura, C., Fukamachi, T., and Sakashita, M.: TCCON data from Saga (JP), Release GGG2014.R0 (Version GGG2014.R0), CaltechDATA [data set], <https://doi.org/10.14291/TCCON.GGG2014.SAGA01.R0/1149283>, 2014.

- Kivi, R., Heikkinen, P., and Kyro, E.: TCCON data from Sodankylä (FI), Release GGG2014.R0 (Version GGG2014.R0), CaltechDATA [data set], <https://doi.org/10.14291/TCCON.GGG2014.SODANKYLA01.R0/1149280>, 2014.
- Lamarque, J.-F., Shindell, D. T., Josse, B., Young, P. J., Cionni, I., Eyring, V., Bergmann, D., Cameron-Smith, P., Collins, W. J., Doherty, R., Dalsoren, S., Faluvegi, G., Folberth, G., Ghan, S. J., Horowitz, L. W., Lee, Y. H., MacKenzie, I. A., Nagashima, T., Naik, V., Plummer, D., Righi, M., Rumbold, S. T., Schulz, M., Skeie, R. B., Stevenson, D. S., Strode, S., Sudo, K., Szopa, S., Voulgarakis, A., and Zeng, G.: The Atmospheric Chemistry and Climate Model Intercomparison Project (ACCMIP): overview and description of models, simulations and climate diagnostics, *Geosci. Model Dev.*, 6, 179–206, <https://doi.org/10.5194/gmd-6-179-2013>, 2013.
- Lambert, G. and Schmidt, S.: Re-evaluation of the oceanic flux of methane: Uncertainties and long-term variations, *Chemosphere*, 26, 579–589, 1993.
- Le Quéré, C., Jackson, R. B., Jones, M. W., Smith, A. J. P., Abernethy, S., Andrew, R. M., De-Gol, A. J., Willis, D. R., Shan, Y., Canadell, J. G., Friedlingstein, P., Creutzig, F., and Peters, G.: Temporary reduction in daily global CO<sub>2</sub> emissions during the COVID-19 forced confinement, *Nat. Clim. Chang.*, 10, 647–653, <https://doi.org/10.1038/s41558-020-0797-x>, 2020.
- Liu, C., Wang, W., and Sun, Y.: TCCON data from Hefei, China, Release GGG2014R0, TCCON data archive, hosted by CaltechDATA, California Institute of Technology, Pasadena, CA, USA [data set], <https://doi.org/10.14291/tcccon.ggg2014.hefei01.R0>, 2018.
- Lopez, M., Schmidt, M., Ramonet, M., Bonne, J.-L., Colomb, A., Kazan, V., Laj, P., and Pichon, J.-M.: Three years of semi-continuous greenhouse gas measurements at the Puy de Dôme station (central France), *Atmos. Meas. Tech.*, 8, 3941–3958, <https://doi.org/10.5194/amt-8-3941-2015>, 2015.
- Makarova, M. V., Kirner, O., Timofeev, Y. M., Poberovskii, A. V., Imkhasin, K. K., Osipov, S. I., and Makarov, B. K.: Analysis of methane total column variations in the atmosphere near St. Petersburg using ground-based measurements and simulations, *Izv. Atmos. Ocean. Phys.*, 51, 177–185, <https://doi.org/10.1134/S0001433815010089>, 2015.
- Masarie, K. A. and Tans, P. P.: Extension and Integration of Atmospheric Carbon Dioxide Data into a Globally Consistent Measurement Record, *J. Geophys. Res.*, 100, 11593–11610, 1995.
- Masarie, K. A., Peters, W., Jacobson, A. R., and Tans, P. P.: ObsPack: a framework for the preparation, delivery, and attribution of atmospheric greenhouse gas measurements, *Earth Syst. Sci. Data*, 6, 375–384, <https://doi.org/10.5194/essd-6-375-2014>, 2014.
- Massart, S., Agustí-Panareda, A., Aben, I., Butz, A., Chevallier, F., Crevoisier, C., Engelen, R., Frankenberg, C., and Hasekamp, O.: Assimilation of atmospheric methane products into the MACC-II system: from SCIAMACHY to TANSO and IASI, *Atmos. Chem. Phys.*, 14, 6139–6158, <https://doi.org/10.5194/acp-14-6139-2014>, 2014.
- Massart, S., Agustí-Panareda, A., Heymann, J., Buchwitz, M., Chevallier, F., Reuter, M., Hilker, M., Burrows, J. P., Deutscher, N. M., Feist, D. G., Hase, F., Sussmann, R., Desmet, F., Dubey, M. K., Griffith, D. W. T., Kivi, R., Petri, C., Schneider, M., and Velazco, V. A.: Ability of the 4-D-Var analysis of the GOSAT BESD XCO<sub>2</sub> retrievals to characterize atmospheric CO<sub>2</sub> at large and synoptic scales, *Atmos. Chem. Phys.*, 16, 1653–1671, <https://doi.org/10.5194/acp-16-1653-2016>, 2016.
- Massart, S., Agustí-Panareda, A., and Flemming, J.: Evidence of a stratospheric methane bias in the IFS against MI-PAS data, ECMWF Technical Memorandum, 814, 21 pp., <https://www.ecmwf.int/sites/default/files/elibrary/2017/17698-evidence-stratospheric-methane-bias-ifs-against-mipas-data.pdf> (last access: 18 March 2023), 2017.
- Matthews, E., Fung, I., and Lerner, J.: Methane emission from rice cultivation: Geographic and seasonal distribution of cultivated areas and emissions, *Global Biogeochem. Cy.*, 5, 3–24, 1991.
- McNorton, J., Bousserez, N., Agustí-Panareda, A., Balsamo, G., Cantarello, L., Engelen, R., Huijnen, V., Inness, A., Kipling, Z., Parrington, M., and Ribas, R.: Quantification of methane emissions from hotspots and during COVID-19 using a global atmospheric inversion, *Atmos. Chem. Phys.*, 22, 5961–5981, <https://doi.org/10.5194/acp-22-5961-2022>, 2022.
- Morino, I., Yokozeki, N., Matsuzaki, T., and Horikawa, M.: TCCON data from Rikubetsu (JP), Release GGG2014.R1 (Version GGG2014.R1), CaltechDATA [data set], <https://doi.org/10.14291/TCCON.GGG2014.RIKUBETSU01.R1/1242265>, 2016a.
- Morino, I., Matsuzaki, T., and Horikawa, M.: TCCON data from Tsukuba (JP), 125HR, Release GGG2014.R1 (Version GGG2014.R1), CaltechDATA [data set], <https://doi.org/10.14291/TCCON.GGG2014.TSUKUBA02.R1/1241486>, 2016b.
- Morino, I., Velazco, V. A., Hori, A., Uchino, O., and Griffith, D. W. T.: TCCON data from Burgos, Philippines, Release GGG2014R0, TCCON data archive, hosted by CaltechDATA, California Institute of Technology, Pasadena, CA, USA [data set], <https://doi.org/10.14291/tcccon.ggg2014.burgos01.R0/1368175>, 2018.
- Necki, J., Schmidt, M., Rozanski, K., Zimnoch, M., Korus, A., Lasa, J., Graul, R., and Levin, I.: Six-year record of atmospheric carbon dioxide and methane at a high-altitude mountain site in Poland, *Tellus B*, 55, 94–104, <https://doi.org/10.1034/j.1600-0889.2003.01446.x>, 2003.
- NOAA Carbon Cycle Group ObsPack Team: Multi-laboratory compilation of atmospheric methane data for the period 1957–2017; *obspack\_ch4\_1\_GLOBALVIEWplus\_v1.0\_2019\_01\_08*, NOAA Earth System Research Laboratory, Global Monitoring Division [data set], <https://doi.org/10.25925/20190108>, 2019.
- Notholt, J., Warneke, T., Petri, C., Deutscher, N. M., Weinzierl, C., Palm, M., and Buschmann, M.: TCCON data from Bremen (DE), Release GGG2014.R0 (Version GGG2014.R0), CaltechDATA [data set], <https://doi.org/10.14291/TCCON.GGG2014.BREMEN01.R0/1149275>, 2014.
- Notholt, J., Warneke, T., Petri, C., Deutscher, N. M., Weinzierl, C., Palm, M., and Buschmann, M.: TCCON data from Ny A°lesund, Spitsbergen (NO), Release GGG2014.R1 (Version R1), CaltechDATA [data set], <https://doi.org/10.14291/TCCON.GGG2014.NYALESEND01.R1>, 2019.
- Olivier, J. and Janssens-Maenhout G.: CO<sub>2</sub> Emissions from Fuel Combustion – 2012 Edition, IEA CO<sub>2</sub> report 2012, Part III, Greenhouse-Gas Emissions, OECD Publishing, Paris, ISBN 978-92-64-17475-7, 2012.

- Ortega, I., Hannigan, J. W., Buchholz, R. R., and Pfister, G.: Long-term variability and source signature of gases emitted from oil & natural gas and cattle feedlot operations in the Colorado front range, *Atmos. Environ.*, 263, 118663, <https://doi.org/10.1016/j.atmosenv.2021.118663>, 2021.
- Patra, P. K., Law, R. M., Peters, W., Rödenbeck, C., Taki-gawa, M., Aulagnier, C., Baker, I., Bergmann, D. J., Bousquet, P., Brandt, J., Bruhwiler, L., Cameron-Smith, P. J., Christensen, J. H., Delage, F., Denning, A. S., Fan, S., Geels, C., Houweling, S., Imasu, R., Karstens, U., Kawa, S. R., Kleist, J., Krol, M., Lin, S.-J., Lokupitiya, R., Maki, T., Maksyutov, S., Niwa, Y., Onishi, R., Parazoo, N., Pieterse, G., Rivier, L., Satoh, M., Serrar, S., Taguchi, S., Vautard, R., Vermeulen, A. T., and Zhu, Z.: TransCom model simulations of hourly atmospheric CO<sub>2</sub>: Analysis of synoptic-scale variations for the period 2002–2003, *Global Biogeochem. Cy.*, 22, GB4013, <https://doi.org/10.1029/2007GB003081>, 2008.
- Patra, P. K., Houweling, S., Krol, M., Bousquet, P., Belikov, D., Bergmann, D., Bian, H., Cameron-Smith, P., Chipperfield, M. P., Corbin, K., Fortems-Cheiney, A., Fraser, A., Gloor, E., Hess, P., Ito, A., Kawa, S. R., Law, R. M., Loh, Z., Maksyutov, S., Meng, L., Palmer, P. I., Prinn, R. G., Rigby, M., Saito, R., and Wilson, C.: TransCom model simulations of CH<sub>4</sub> and related species: linking transport, surface flux and chemical loss with CH<sub>4</sub> variability in the troposphere and lower stratosphere, *Atmos. Chem. Phys.*, 11, 12813–12837, <https://doi.org/10.5194/acp-11-12813-2011>, 2011.
- Peterson, J. T., Komhyr, W. D., Waterman, L. S., Gammon, R. H., Thoning, K. W., and Conway, T. J.: Atmospheric CO<sub>2</sub> variations at Barrow, Alaska, 1973–1982, *J. Atmos. Chem.*, 4, 491–510, 1986.
- Petri, C., Rousogenous, C., Warneke, T., Vrekoussis, M., Sciare, S., and Notholt, J.: TCCON data from Nicosia, Cyprus, Release GGG2014R0, TCCON data archive, hosted by CaltechDATA, California Institute of Technology, Pasadena, CA, USA [data set], <https://doi.org/10.14291/tccon.ggg2014.nicosia01.R0>, 2020.
- Pollard, D., Robinson, J., and Shiona, H.: TCCON data from Lauder (NZ), Release GGG2014.R0 (GGG2014.R0), CaltechDATA [data set], <https://doi.org/10.14291/tccon.ggg2014.lauder03.R0>, 2019.
- Pollard, D. F., Sherlock, V., Robinson, J., Deutscher, N. M., Connor, B., and Shiona, H.: The Total Carbon Column Observing Network site description for Lauder, New Zealand, *Earth Syst. Sci. Data*, 9, 977–992, <https://doi.org/10.5194/essd-9-977-2017>, 2017.
- Ramonet, M. and Monfray, P.: CO<sub>2</sub> baseline concept in 3-D atmospheric transport models, *Tellus B*, 48, 502–520, 1996.
- Ramonet, M., Ciais, P., Aalto, T., Aulagnier, C., Chevallier, F., Cipriano, D., Conway, T. J., Haszpra, L., Kazan, V., Meinhardt, F., Paris, J.-D., Schmidt, M., Simmonds, P., Xueref-Remy, I., and Necki, J.: A recent build-up of atmospheric CO<sub>2</sub> over Europe. Part 1: observed signals and possible explanations, *Tellus B*, 62, 1–13, <https://doi.org/10.1111/j.1600-0889.2009.00442.x>, 2010.
- Reuter, M., Bovensmann, H., Buchwitz, M., Burrows, J. P., Connor, B. J., Deutscher, N. M., Griffith, D. W. T., Heymann, J., Keppel-Aleks, G., Messerschmidt, J., Notholt, J., Petri, C., Robinson, J., Schneising, O., Sherlock, V., Velazco, V., Warneke, W., Wennberg, P. O., and Wunch, D.: Retrieval of atmospheric CO<sub>2</sub> with enhanced accuracy and precision from SCIAMACHY: Validation with FTS measurements and comparison with model results, *J. Geophys. Res.*, 116, D04301, <https://doi.org/10.1029/2010JD015047>, 2011.
- Ridgwell, A. J., Marshall, S. J., and Gregson, K.: Consumption of atmospheric methane by soils: A process-based model, *Global Biogeochem. Cy.*, 13, 59–70, <https://doi.org/10.1029/1998GB900004>, 1999.
- Rodgers, C. D.: Inverse Methods for Atmospheric Sounding: Theory and Practice, World Scientific, <https://doi.org/10.1142/3171>, 2000.
- Sanderson, M. G.: Biomass of termites and their emissions of methane and carbon dioxide: A global database, *Global Biogeochem. Cy.*, 10, 543–557, 1996.
- Sandu, I., Beljaars, A., Bechtold, P., Mauritsen, T., and Balsamo, G.: Why is it so difficult to represent stably stratified conditions in numerical weather prediction (NWP) models?, *J. Adv. Model. Earth Sy.*, 5, 117–133, 2013.
- Schepers, D., Guerlet, S., Butz, A., Landgraf, J., Frankenberg, C., Hasekamp, O., Blavier, J.-F., Deutscher, N. M., Griffith, D. W. T., Hase, F., Kyro, E., Morino, I., Sherlock, V., Sussmann, R., and Aben, I.: Methane retrievals from Greenhouse Gases Observing Satellite (GOSAT) shortwave infrared measurements: Performance comparison of proxy and physics retrieval algorithms, *J. Geophys. Res.-Atmos.*, 117, D10307, <https://doi.org/10.1029/2012JD017549>, 2012.
- Schepers, D. A., Butz, H. H., Hasekamp, O. P., Arnold, S. G., Schneider, M., Feist, D. G., Morino, I., Pollard, D., Aben, I., and Landgraf, J.: Methane and carbon dioxide total column retrievals from cloudy GOSAT soundings over the oceans, *J. Geophys. Res.-Atmos.*, 121, 5031–5050, <https://doi.org/10.1002/2015JD023389>, 2016.
- Schmidt, M., Graul, R., Sartorius, H., and Levin, L.: The Schauinsland CO<sub>2</sub> record: 30 years of continental observations and their implications for the variability of the European CO<sub>2</sub> budget, *J. Geophys. Res.-Atmos.*, 108, 4619–4626, 2003.
- Schuldt, K., Mund, J., Luijckx, I. T., Jacobson, A. R., Aalto, T., Abshire, J. B., Aikin, K., Andrews, A., Aoki, S., Apadula, F., Baier, B., Bakwin, P., Bartyzel, J., Bentz, G., Bergamaschi, P., Beyersdorf, A., Biermann, T., Biraud, S. C., Bowling, D., Brailsford, G., Chen, G., Chen, H., Chmura, L., Clark, S., Colomb, A., Commane, R., Conil, S., Cox, A., Cristofanelli, P., Cuevas, E., Curcoll, R., Daube, B., Davis, K., De Mazière, M., De Wekker, S., Della Coletta, J., Delmotte, M., DiGangi, J. P., Dlugokencky, E., Elkins, J. W., Emmenegger, L., Fischer, M. L., Forster, G., Frumau, A., Galkowski, M., Gatti, L. V., Gheusi, F., Gloor, E., Gomez-Trueba, V., Goto, D., Griffis, T., Hammer, S., Hanson, C., Haszpra, L., Hatakka, J., Heliasz, M., Hensen, A., Hermanssen, O., Hintsa, E., Holst, J., Jaffe, D., Joubert, W., Karion, A., Kawa, S. R., Keeling, R., Keronen, P., Kolari, P., Kominkova, K., Kort, E., Krummel, P., Kubistin, D., Labuschagne, C., Langenfelds, R., Laurent, O., Laurila, T., Lauvaux, T., Law, B., Lee, J., Lehner, I., Leuenberger, M., Levin, I., Levula, J., Lin, J., Lindauer, M., Loh, Z., Lopez, M., Machida, T., Mammarella, I., Manca, G., Manning, A., Manning, A., Marek, M. V., Martin, M. Y., Mat-sueda, H., McKain, K., Meijer, H., Meinhardt, F., Merchant, L., Mihalopoulos, N., Miles, N., Miller, J. B., Miller, C. E., Mitchell, L., Montzka, S., Moore, F., Morgan, E., Morgui, J. A., Morimoto, S., Munger, B., Myhre, C. L., Mölder, M., Müller-Williams,

- J., Necki, J., Newman, S., Nichol, S., Niwa, Y., O'Doherty, S., Paplawsky, B., Peischl, J., Peltola, O., Pichon, J. M., Piper, S., Plass-Duelmer, C., Ramonet, M., Ramos, R., Reyes-Sanchez, E., Richardson, S., Riris, H., Rivas, P. P., Ryerson, T., Saito, K., Sargent, M., Sawa, Y., Say, D., Scheeren, B., Schmidt, M., Schumacher, M., Sha, M. K., Shepson, P., Shook, M., Sloop, C. D., Smith, P., Steinbacher, M., Stephens, B., Sweeney, C., Tans, P., Thoning, K., Torn, M., Trisolino, P., Turnbull, J., Tørseth, K., Vermeulen, A., Viner, B., Vitkova, G., Walker, S., Weyrauch, D., Wofsy, S., Worthy, D., Young, D., Zimnoch, M., van Dinther, D., and van den Bulk, P.: Multi-laboratory compilation of atmospheric carbon dioxide data for the period 1957–2019; obspack\_co2\_1\_GLOBALVIEWplus\_v6.0\_2020-09-11, NOAA Earth System Research Laboratory, Global Monitoring Division [data set], <https://doi.org/10.25925/20200903>, 2020.
- Schuldt, K. N., Jacobson, A. R., Aalto, T., Andrews, A., Bakwin, P., Bergamaschi, P., Biermann, T., Biraud, S. C., Chen, H., Colomb, A., Conil, S., Cristofanelli, P., De Mazière, M., De Wekker, S., Delmotte, M., Dlugokencky, E., Emmenegger, L., Fischer, M. L., Hatakka, J., Heliasz, M., Hermanssen, O., Holst, J., Jaffe, D., Karion, A., Kazan, V., Keronen, P., Kominkova, K., Kubistin, D., Laurent, O., Laurila, T., Lee, J., Lehner, I., Leuenberger, M., Lindauer, M., Lopez, M., Mammarella, I., Manca, G., Marek, M. V., McKain, K., Miller, J. B., Miller, C. E., Myhre, C. L., Mölder, M., Müller-Williams, J., Piacentino, S., Pichon, J. M., Plass-Duelmer, C., Ramonet, M., Scheeren, B., Schumacher, M., Sha, M. K., Sloop, C. D., Smith, P., Steinbacher, M., Sweeney, C., Tans, P., Thoning, K., Trisolino, P., Tørseth, K., Viner, B., Vitkova, G., and di Sarra, A. G.: Multi-laboratory compilation of atmospheric carbon dioxide data for the period 2020–2021; obspack\_co2\_1\_NRT\_v6.1\_2021-02-02, NOAA Earth System Research Laboratory, Global Monitoring Laboratory [data set], <https://doi.org/10.25925/20210108>, 2021.
- Segers, A., Tokaya, J., and Houweling, S.: Description of the CH<sub>4</sub> Inversion Production Chain, Copernicus Atmosphere Monitoring Service, [https://atmosphere.copernicus.eu/sites/default/files/2021-01/CAMS73\\_2018SC3\\_D73.5.2.2-2020\\_202012\\_production\\_chain\\_Ver1.pdf](https://atmosphere.copernicus.eu/sites/default/files/2021-01/CAMS73_2018SC3_D73.5.2.2-2020_202012_production_chain_Ver1.pdf) (last access: 18 March 2023), 2020a.
- Segers, A., Tokaya, J., and Houweling, S.: Validation of the CH<sub>4</sub> surface flux inversion – reanalysis 1990–2019, Copernicus Atmosphere Monitoring Service EQC report, Dec 2020, [https://atmosphere.copernicus.eu/sites/default/files/2021-02/CAMS73\\_2018SC2\\_D73.2.4.1-2020\\_202012\\_validation\\_CH4\\_1990-2019\\_v2.pdf](https://atmosphere.copernicus.eu/sites/default/files/2021-02/CAMS73_2018SC2_D73.2.4.1-2020_202012_validation_CH4_1990-2019_v2.pdf) (last access: 18 March 2023), 2020b.
- Sha, M. K., Langerock, B., Blavier, J.-F. L., Blumenstock, T., Borsdorff, T., Buschmann, M., Dehn, A., De Mazière, M., Deutscher, N. M., Feist, D. G., García, O. E., Griffith, D. W. T., Grutter, M., Hannigan, J. W., Hase, F., Heikkinen, P., Hermans, C., Iraci, L. T., Jeseck, P., Jones, N., Kivi, R., Kumps, N., Landgraf, J., Lorente, A., Mahieu, E., Makarova, M. V., Mellqvist, J., Metzger, J.-M., Morino, I., Nagahama, T., Notholt, J., Ohyama, H., Ortega, I., Palm, M., Petri, C., Pollard, D. F., Rettinger, M., Robinson, J., Roche, S., Roehl, C. M., Röhling, A. N., Rousogenous, C., Schneider, M., Shiomi, K., Smale, D., Stremme, W., Strong, K., Sussmann, R., Té, Y., Uchino, O., Velazco, V. A., Vigouroux, C., Vrekoussis, M., Wang, P., Warneke, T., Wittenberg, T., Wunch, D., Yamanouchi, S., Yang, Y., and Zhou, M.: Validation of methane and carbon monoxide from Sentinel-5 Precursor using TCCON and NDACC-IRWG stations, *Atmos. Meas. Tech.*, 14, 6249–6304, <https://doi.org/10.5194/amt-14-6249-2021>, 2021.
- Sherlock, V., Connor, B., Robinson, J., Shiona, H., Smale, D., and Pollard, D. F.: TCCON data from Lauder (NZ), 125HR, Release GGG2014.R0 (Version GGG2014.R0), CaltechDATA [data set], <https://doi.org/10.14291/tcon.ggg2014.lauder02.R0/1149298>, 2014a.
- Sherlock, V., Connor, B., Robinson, J., Shiona, H., Smale, D., and Pollard, D.: TCCON data from Lauder, New Zealand, 120HR, Release GGG2014R0, CaltechDATA [data set], <https://doi.org/10.14291/tcon.ggg2014.lauder01.R0/1149293>, 2014b.
- Spahni, R., Wania, R., Neef, L., van Weele, M., Pison, I., Bousquet, P., Frankenberg, C., Foster, P. N., Joos, F., Prentice, I. C., and van Velthoven, P.: Constraining global methane emissions and uptake by ecosystems, *Biogeosciences*, 8, 1643–1665, <https://doi.org/10.5194/bg-8-1643-2011>, 2011.
- Stephens, B. B., Brailsford, G. W., Gomez, A. J., Riedel, K., Mikaloff Fletcher, S. E., Nichol, S., and Manning, M.: Analysis of a 39-year continuous atmospheric CO<sub>2</sub> record from Baring Head, New Zealand, *Biogeosciences*, 10, 2683–2697, <https://doi.org/10.5194/bg-10-2683-2013>, 2013.
- Stevenson, D. S., Derwent, R. G., Wild, O., and Collins, W. J.: COVID-19 lockdown emission reductions have the potential to explain over half of the coincident increase in global atmospheric methane, *Atmos. Chem. Phys.*, 22, 14243–14252, <https://doi.org/10.5194/acp-22-14243-2022>, 2022.
- Strong, K., Roche, S., Franklin, J. E., Mendonca, J., Lutsch, E., Weaver, D., Fogal, P. F., Drummond, J. R., Batchelor, R., and Lindenmaier, R.: TCCON data from Eureka (CA), Release GGG2014.R3 (Version R3), CaltechDATA [data set], <https://doi.org/10.14291/TCCON.GGG2014.EUREKA01.R3>, 2019.
- Sussmann, R. and Rettinger, M.: TCCON data from Garmisch (DE), Release GGG2014.R2 (Version R2), CaltechDATA [data set], <https://doi.org/10.14291/TCCON.GGG2014.GARMISCH01.R2>, 2018a.
- Sussmann, R. and Rettinger, M.: TCCON data from Zugspitze, Germany, Release GGG2014R1, TCCON data archive, hosted by CaltechDATA, California Institute of Technology, Pasadena, CA, USA [data set], <https://doi.org/10.14291/tcon.ggg2014.zugspitze01.R1>, 2018b.
- Sussmann, R., Forster, F., Rettinger, M., and Bousquet, P.: Renewed methane increase for five years (2007–2011) observed by solar FTIR spectrometry, *Atmos. Chem. Phys.*, 12, 4885–4891, <https://doi.org/10.5194/acp-12-4885-2012>, 2012.
- Sussmann, R., Ostler, A., Forster, F., Rettinger, M., Deutscher, N. M., Griffith, D. W. T., Hannigan, J. W., Jones, N., and Patra, P. K.: First intercalibration of column-averaged methane from the Total Carbon Column Observing Network and the Network for the Detection of Atmospheric Composition Change, *Atmos. Meas. Tech.*, 6, 397–418, <https://doi.org/10.5194/amt-6-397-2013>, 2013.
- Takahashi, T., Sutherland, S. C., Wanninkhof, R., Sweeney, C., Feely, R. A., Chipman, D. W., Hales, B., Friederich, G., Chavez, F., Sabine, C., Watson, A., Bakker, D., Schuster, U., Metzl, N., Yoshikawa-Inoue, H., Ishii, M., Midorikawa, T., Nojiri, Y., Körtzinger, A., Steinhoff, T., Hoppema, M., Olafsson, J., Arnarson, T. S., Tilbrook, B., Jhannessen, T., Olsen, A., Bellerby, R., Wong, C. S., Delille, B., Bates, N. R., and de Baar, H. J. W.: Cli-

- matological mean and decadal change in surface ocean pCO<sub>2</sub>, and net sea–air CO<sub>2</sub> flux over the global oceans, *Deep Sea Res. Pt. II*, 56, 554–577, 2009.
- Te, Y., Jeseck, P., and Janssen, C.: TCCON data from Paris (FR), Release GGG2014.R0 (Version GGG2014.R0), CaltechDATA [data set], <https://doi.org/10.14291/TCCON.GGG2014.PARIS01.R0/1149279>, 2014.
- Temperton, C., Hortal, M., and Simmons, A. A.: two-time-level semi-Lagrangian global spectral model, *Q. J. Roy. Meteor. Soc.*, 127, 111–127, 2001.
- Tsutsumi, Y., Matsueda, H., and Nishioka, S.: Consistency of the CO<sub>2</sub> primary standards in JMA, 12th WMO/IAEA meeting of experts on carbon dioxide concentration and related tracers measurement techniques, Toronto, Canada, 15–18 September 2003, Global Atmosphere Watch Report No. 161 (WMO/TD-No.1275), 23–31, 2005.
- Verma, S., Marshall, J., Parrington, M., Agustí-Panareda, A., Massart, S., Chipperfield, M. P., Wilson, C., and Gerbig, C.: Extending methane profiles from aircraft into the stratosphere for satellite total column validation using the ECMWF C-IFS and TOMCAT/SLIMCAT 3-D model, *Atmos. Chem. Phys.*, 17, 6663–6678, <https://doi.org/10.5194/acp-17-6663-2017>, 2017.
- Warneke, T., Messerschmidt, J., Notholt, J., Weinzierl, C., Deutscher, N. M., Petri, C., and Grupe, P.: TCCON data from Orleåns (FR), Release GGG2014.R0 (Version GGG2014.R0), CaltechDATA [data set], <https://doi.org/10.14291/TCCON.GGG2014.ORLEANS01.R0/1149276>, 2014.
- Waterman, L. S., Nelson, D. W., Komhyr, W. D., Harris, T. B., and Thoning, K. W.: Atmospheric carbon dioxide measurements at Cape Matatula, American Samoa, 1976–1984, *J. Geophys. Res.*, 94, 14817–14829, 1989.
- Wennberg, P. O., Wunch, D., Roehl, C. M., Blavier, J.-F., Toon, G. C., and Allen, N. T.: TCCON data from Caltech (US), Release GGG2014.R1 (Version GGG2014.R1), CaltechDATA [data set], <https://doi.org/10.14291/TCCON.GGG2014.PASADENA01.R1/1182415>, 2015.
- Wennberg, P. O., Wunch, D., Roehl, C. M., Blavier, J.-F., Toon, G. C., and Allen, N. T.: TCCON data from Lamont (US), Release GGG2014.R1 (Version GGG2014.R1), CaltechDATA [data set], <https://doi.org/10.14291/TCCON.GGG2014.LAMONT01.R1/1255070>, 2016a.
- Wennberg, P. O., Wunch, D., Yavin, Y., Toon, G. C., Blavier, J.-F., Allen, N., and Keppel-Aleks, G.: TCCON data from Jet Propulsion Laboratory, Pasadena, California, USA, Release GGG2014R0, TCCON data archive, hosted by CaltechDATA, California Institute of Technology, Pasadena, CA, USA [data set], <https://doi.org/10.14291/tcccon.ggg2014.jpl01.R0/1149163>, 2016b.
- Wennberg, P. O., Roehl, C. M., Wunch, D., Toon, G. C., Blavier, J.-F., Washenfelder, R., Keppel-Aleks, G., Allen, N. T., and Ayers, J.: TCCON data from Park Falls (US), Release GGG2014.R1 (Version GGG2014.R1), CaltechDATA [data set], <https://doi.org/10.14291/TCCON.GGG2014.PARKFALLS01.R1>, 2017.
- Williams, J. E., Huijnen, V., Bouarar, I., Meziane, M., Schreurs, T., Pelletier, S., Marécal, V., Josse, B., and Flemming, J.: Regional evaluation of the performance of the global CAMS chemical modeling system over the United States (IFS cycle 47r1), *Geosci. Model Dev.*, 15, 4657–4687, <https://doi.org/10.5194/gmd-15-4657-2022>, 2022.
- Worthy, D. E., Higuchi, K., and Chan, D.: North American influence on atmospheric carbon dioxide data collected at Sable Island, Canada, *Tellus*, 55B, 105–114, 2003.
- Wunch, D., Toon, G. C., Blavier, J.-F. L., Washenfelder, R. A., Notholt, J., Connor, B. J., Griffith, D. W. T., Sherlock, V., and Wennberg, P. O.: The Total Carbon Column Observing Network, *Philos. Trans. R. Soc. A Math. Phys. Eng. Sci.*, 369, 2087–2112, <https://doi.org/10.1098/rsta.2010.0240>, 2011.
- Wunch, D., Toon, G. C., Sherlock, V., Deutscher, N. M., Liu, C., Feist, D. G., and Wennberg, P. O.: The Total Carbon Column Observing Network's GGG2014 Data Version, Pasadena, California, 2015.
- Wunch, D., Mendonca, J., Colebatch, O., Allen, N. T., Blavier, J.-F., Roche, S., Hedelius, J., Neufeld, G., Springett, S., Worthy, D., Kessler, R., and Strong, K.: TCCON data from East Trout Lake, Canada, Release GGG2014R1, TCCON data archive, hosted by CaltechDATA, California Institute of Technology, Pasadena, CA, USA [data set], <https://doi.org/10.14291/tcccon.ggg2014.easttroutlake01.R1>, 2018.
- Zander, R., Mahieu, E., Demoulin, P., Duchatelet, P., Roland, G., Servais, C., Mazière, M., De Reimann, S., and Rinsland, C. P.: Our changing atmosphere: Evidence based on long-term infrared solar observations at the Jungfraujoch since 1950, *Sci. Total Environ.*, 391, 184–195, <https://doi.org/10.1016/j.scitotenv.2007.10.018>, 2008.
- Zhou, M., Langerock, B., Vigouroux, C., Sha, M. K., Ramonet, M., Delmotte, M., Mahieu, E., Bader, W., Hermans, C., Kumps, N., Metzger, J.-M., Duflat, V., Wang, Z., Palm, M., and De Mazière, M.: Atmospheric CO and CH<sub>4</sub> time series and seasonal variations on Reunion Island from ground-based in situ and FTIR (NDACC and TCCON) measurements, *Atmos. Chem. Phys.*, 18, 13881–13901, <https://doi.org/10.5194/acp-18-13881-2018>, 2018.